Role of iron and cobalt in 4-component Bi-Mo-Co-Fe-O catalysts for selective isobutene oxidation using complementary *operando* techniques

Linda Klag[1], Abhijeet Gaur[1], Matthias Stehle[1], Sebastian Weber[2], Thomas L. Sheppard[1,2,†], Jan-Dierk Grunwaldt[1,2,]*

[1]Institute for Chemical Technology and Polymer Chemistry (ITCP), Karlsruhe Institute of Technology (KIT), 76131 Karlsruhe, Germany

[2]Institute of Catalysis Research and Technology (IKFT), Karlsruhe Institute of Technology (KIT), 76344 Eggenstein-Leopoldshafen, Germany

[†]Current address: Institute of Chemical Technology, Leipzig University, 04103 Leipzig, Germany

*Corresponding author: grunwaldt@kit.edu

Abstract

Structure-activity correlations in the selective oxidation of lower olefins over Bi-Mo-based mixed metal oxides are challenging but essential for a knowledge-based catalyst design and improvement of process efficiency. One important aspect is the extension of the 2-component Bi-Mo-oxides to more complex mixed metal oxide (MMO) systems like Bi-Mo-Co-Fe-oxides, as their higher activity and selectivity is traced back to synergistic metal oxide phase interactions. Hence, three Bi-Mo-Co-Fe-oxide catalysts differing in elemental composition, especially iron and cobalt content, were tested during the selective oxidation of isobutene. The catalyst structure was studied using *operando* Raman spectroscopy, (synchrotron) X-ray diffraction and X-ray absorption spectroscopy. The formation of ternary phases β-$Co_{0.7}Fe_{0.3}MoO_4$ and $Bi_3FeMo_2O_{12}$ resulted in an increased selectivity to methacrolein, but the overall performance strongly depended on the variety of metal oxide phases and thus points to the role of phase cooperation. The highest selectivity was observed with simultaneous presence of α-$Bi_2Mo_3O_{12}$, while the interplay of γ-Bi_2MoO_6 and Fe_3O_4 led to highly active but less selective catalysts. In this context, the reducibility of Fe^{3+} to Fe^{2+} was found to be crucial for a moderate and controllable catalytic activity. Co_3O_4 performed unselective by mainly favouring total oxidation product formation. Comparison with previous findings in selective propylene oxidation showed similar structural changes during catalytic reaction, hence, emphasizing similar behaviour of Bi-Mo-Co-Fe-oxides in lower olefin oxidation. The systematic investigation of 4-component catalysts by advanced characterization techniques is a powerful approach to gain new insights into the roles of individual catalyst phases by considering their complex phase interplay and thus receiving more profound understanding of their working principles during the selective oxidation of olefins.

Keywords: Selective oxidation, isobutene, methacrolein, mixed metal oxides, *operando*, X-ray diffraction, X-ray absorption spectroscopy, Raman spectroscopy.

1 Introduction

The selective oxidation of propylene and isobutene are key reactions in chemical industry for the functionalization of hydrocarbons, leading to various important intermediates such as acrolein and methacrolein (MAC).[1-3] Both reactions are typically catalyzed by bismuth-molybdate based multicomponent systems, which have been developed over the past decades mainly by trial and error.[4-5] At the same time, research has focused on investigating structure-activity correlations of more simplified model systems (*e.g.*, 2-component Bi-Mo-O) to further improve the efficiency of selective olefin oxidation by gaining a fundamental understanding of their working principles.[6-10] This resulted in various new insights, but also several controversial discussions on the role of individual metal oxide phases during selective olefin oxidation.[11] For example, 4-component Bi-Mo-Co-Fe-O systems are known to be more selective than model 2-component Bi-Mo-O systems, and different activity and selectivity trends were found for the corresponding main phases α-$Bi_2Mo_3O_{12}$, β-$Bi_2Mo_2O_9$ and γ-Bi_2MoO_6.[12-14] These are further related to the strong dependence of catalytic performance on the conditions applied during catalyst preparation or the catalytic reaction itself such as temperature, pressure or gas atmosphere.[15-16] Typical reaction conditions for selective olefin oxidation involve a mixture of propylene/isobutene, air and steam,[1] with water likely influencing both the chemical and physical properties (*e.g.*, heat transfer) in the catalytic process.[11] This underlines both the sensitivity and complexity of (mixed) metal oxide catalysts regarding synthesis or reaction conditions, and the resulting challenge of studying such complex catalysts systematically in a representative manner.

While bismuth molybdates are typically considered as the key active phase in selective olefin oxidation, their catalytic performance can be significantly increased if intermixed or combined with further metals.[9, 17-21] Consequently, modern commercial catalysts consist of complex mixed

metal oxide compositions, generally described with Mo-Bi-M^{II}-M^{III}-M^{I}-X-Y-O (*e.g.*, M^{II}=Co, Ni; M^{III}=Fe, Cr; M^{I}=Na, K; X=Sb, Te; Y=P, B), as reviewed by Moro-Oka and Ueda.[4] Particularly, the first four metals (*e.g.*, Bi-Mo-Co-Fe-O) form the essential structure of the catalyst, mainly influencing catalytic activity and selectivity. Corresponding metal amounts typically include 50-55 at.% Mo, 3-7 at.% Bi, 30-35 at.% Co and 8-15 at.% Fe.[4] In this context, Ueda *et al.* found the catalyst $Mo_{12}Bi_1Co_8Fe_3O_x$ to perform especially well in terms of activity and selectivity during propylene oxidation, compared to other 2-, 3- or 4-component systems.[4] This was attributed to the presence of α- and β-$CoMoO_4$, α-$Bi_2Mo_3O_{12}$, $Fe_2Mo_3O_{12}$, $FeMoO_4$ and MoO_3. However, no definite conclusions on the role of the individual phases and corresponding synergistic phase interactions could be drawn. Thus, it is still not fully understood why this particular catalyst composition shows such high catalytic performance during propylene oxidation compared to other Bi-Mo-Co-Fe-oxides because it is challenging to identify all crystalline and amorphous phases present, including minority phases. In fact, most literature studies have focused on (laboratory-based) *ex situ* characterization of the bismuth molybdate-based catalysts before and after catalytic reaction. In general, only a few studies tackled the more complex multicomponent systems, despite their superior catalytic performance.[22-24] Moreover, the bulk structure of the mixed metal oxides was found an important trigger for the surface structures.[25] Strikingly, the characterization toolbox could recently be extended by various improvements in synchrotron-based and *operando* techniques.[26] In this context, the Bi-Mo-Co-Fe-O catalyst system was investigated *in situ*/*operando* during selective propylene oxidation, gaining first insights into metal oxide phase (trans-) formations and phase amounts in complex 4-component systems.[27] For example, an outstanding performance of $Mo_{12}Bi_1Co_8Fe_3O_x$ including the formation of ternary β-$Co_{0.7}Fe_{0.3}MoO_4$ and $Bi_3FeMo_2O_{12}$ and their synergistic interplay with α-$Bi_2Mo_3O_{12}$ was found.

In addition, MoO_3 was only beneficial in certain amounts and if further incorporated in other phases, but not when isolated.

As a next step regarding a fundamental understanding of the selective olefin oxidation, we now focus on a systematic structural study with isobutene as feedstock, which leads to other valuable products like methacrolein and methacrylic acid. Although various studies and patents claim that the selective oxidation of isobutene to methacrolein is similar to propylene oxidation,[1, 28] only very few fundamental studies have actually addressed selective isobutene oxidation over multicomponent systems,[29-32] resulting in a knowledge gap for this reaction. This might be attributed to the increasing reactivity (and thus complexity) of the selective oxidation with an additional methyl group present. Udalova *et al.* investigated selective isobutene oxidation over several bismuth molybdate-based catalysts (*e.g.*, Co-Mo-Bi-Fe-Sb-K-O) and found the main phases of the Bi-Mo-Co-Fe-O systems to be similar to those previously reported for propylene oxidation.[33] Still, the results only referred to conventional *ex situ* characterization of the catalysts before and after catalytic reaction. Hence, structural changes were not monitored under reaction conditions and thus, the roles of particular metal oxide phases on catalytic activity and selectivity during selective isobutene oxidation are not entirely clarified yet.

To probe parallels and similar selectivity patterns between lower olefins, we investigated the structural evolution of three selected Bi-Mo-Co-Fe-O catalysts during selective isobutene oxidation by using complementary and advanced bulk characterization techniques. The aim was to reveal the role and interaction of the individual metal oxide phases in superior 4-component catalysts by investigating the influence of catalyst composition on activity and selectivity. The catalysts were prepared by flame-spray pyrolysis (FSP) as this single step route provides controlled access to nanocrystalline metal oxide phases with high surface area and defined, homogeneous

metal oxide phase distribution.[24, 34-35] Besides the synthesis of the highly active and selective catalyst composition known from propylene oxidation[17, 27] (denoted as: FSP-U, and used as reference for direct comparison between propylene and isobutene), we focused on two additional catalysts with higher amounts of cobalt (denoted as: FSP-Co) and iron (denoted as: FSP-Fe), and thus lower molybdenum content that were not reported before. Their complex amorphous and crystalline phase ensemble was deconvoluted by complementary *operando* Raman spectroscopy, synchrotron-based X-ray absorption spectroscopy (XAS) and synchrotron-based X-ray diffraction (XRD) with Rietveld refinement. By combining catalytic performance in a lab-scale reactor and *operando* studies in a spectroscopic microreactor, a detailed understanding of the complex phase composition and the potential phase interplay under reaction conditions was obtained. Overall, this step towards increased complexity allowed us to shed light into the role of particular metal oxide phases during selective olefin oxidation and thus their impact on the activity and selectivity under more application-related conditions.

2 Experimental

2.1 Catalyst synthesis

Three Bi-Mo-Co-Fe-O catalysts differing in their elemental composition (**see Table 1**) were synthesized in a single step *via* flame spray pyrolysis (FSP) using the same setup as in our previous studies.[16, 24, 27] FSP-Co and FSP-Fe contained the highest amount of cobalt and iron of 40 mol%, respectively, while FSP-U referred to an elemental composition firstly reported by Moro-Oka and Ueda.[4] The catalyst precursors bismuth(III) acetate ($Bi(OAc)_3$, Sigma Aldrich), bis(2,4-pentanedionato)molybdenum(VI) dioxide ($MoO_2(acac)_2$, Alfa Aesar), cobalt(II) nitrate hexahydrate ($Co(NO_3)_2 \cdot 6H_2O$, Merck) and tris(2,4-pentanedionato)iron(III) ($Fe(acac)_3$, Fluka

Chemika) were dissolved in a 3/2 mixture (v/v) of methanol (MeOH, ≥ 99.9%, VWR chemicals) and acetic acid (HOAc, 99-100%, Sigma Aldrich) to give a 250 mL solution with total precursor concentration of 0.30 M metal content. The procedure was similar to a previously described one,[27] using the precursor masses listed in **Table 1**. The precursor solutions were prepared, transferred into syringes and sprayed through a flame. The obtained powder was collected on a glass fibre filter positioned above the flame and scratched off afterwards. The so-prepared catalysts were calcined for 5 h at 500 °C in static air unless stated elsewhere.

2.2 *Ex situ* characterization

The catalysts were characterised by inductively coupled plasma optical emission spectrometry (ICP-OES) and N_2-physisorption before and after catalytic testing, as well as by laboratory XRD and Raman spectroscopy prior to catalytic testing and SEM-EDX after catalytic testing.

The elemental composition was determined *via* ICP-OES with an iCAP 7600 DUO (Thermo Fisher Scientific) after dissolving 50 mg sample in 6 mL HCl, 2 mL HNO_3 and 1 mL H_2O_2 through heating in a microwave for 45 min at 600 W. The specific surface area of the catalysts was determined by N_2-physisorption at -196 °C using an Autosorb iQ (Quantachrome) and calculated *via* the Brunauer-Emmett-Teller (BET) method[36] in the p/p_0 = 0.05-0.3 range. Prior to the measurements, the samples were heated in vacuum at 150 °C for 3 h. Laboratory powder X-ray diffraction was performed on a PANalytical X'pert Pro diffractometer equipped with Ni-filtered Cu K_α radiation (λ = 1.54060 Å) for 2θ = 5-120° (0.017° steps with 60 s per step). Phase assignment was carried out using the Inorganic Crystal Structure Database (ICSD). *Ex situ* Raman spectroscopy was measured with an inVia Raman spectrometer (Renishaw) equipped with a frequency doubled Nd:YAG laser (532 nm, 100 mW) and an optical microscope (Leica).

Table 1. Metal ratios (as calculated) and precursor masses used for FSP with corresponding specific surface area (A_{BET}) of the calcined catalysts before and after catalytic testing as determined by N_2-physisorption.

Sample	Metal ratio / mol%				Precursor mass / g				A_{BET} / m^2 g^{-1}	
	Bi	Mo	Co	Fe	$Bi(OAc)_3$	$MoO_2(acac)_2$	$Co(NO_3)_2 \cdot 6H_2O$	$Fe(acac)_3$	before	after
FSP-Co	5.0	35.0	40.0	20.0	1.45	8.56	8.73	5.30	34	19
FSP-Fe	5.0	35.0	20.0	40.0	1.45	8.56	4.37	10.60	32	21
FSP-U	4.2	50.0	33.3	12.5	1.22	12.23	7.27	3.31	15	13

For additional material properties see **SI, section 1**.

An area of at least 200 x 150 μm^2 (~20.000 spectra) with a raster size of 1.3 µm was scanned using a line shaped laser (1% laser intensity, 30 s acquisition time, 2400 lines/mm grating, spectral range of 60-1320 cm^{-1}). Data treatment including cosmic ray removal, noise filtering, truncation, baseline subtraction and averaging was done with the software WiRE 4.4 (Renishaw). SEM-EDX measurements were conducted with a Gemini SEM 500 (Zeiss) at 10 kV, and an Oxford X-Max^N EDX system (Oxford Instruments).

2.3 Catalytic testing

The integral catalytic performance in selective isobutene oxidation was determined in a fixed-bed testing unit with an on-line gas chromatograph (GC) for product analysis. This setup is described in detail in literature[16] and additional information is given in **SI section 2.1**. The calcined catalysts FSP-Co, FSP-Fe and FSP-U were ground, then pressed and sieved to give a sieve fraction of 300-450 µm. 100 mg of the sieve fraction was diluted with 500 mg SiC (450-600 µm) to avoid thermal runaway and placed in a tubular quartz reactor. First, all catalysts were heated to 180 °C (5 °C/min) in synthetic air (N_2/O_2 = 80/20 vol.%, 100 mL/min) for preconditioning. Afterwards, each catalyst was heated stepwise up to the respective ignition temperature (T_{oven} = 400 °C, 440 °C or 490 °C, 2 °C/min) under reaction conditions ($N_2/O_2/C_4H_8/H_2O$ = 70/14/8/8 vol%, ~1 atm). The total flow was set to 50, 75, 100 and 150 mL/min in order to probe different weight hourly space velocities (WHSV) from 6.2-18.7 h^{-1}. For each condition, the oven temperature and WHSV were kept constant for at least 3 h until a stable conversion level was achieved as monitored by an on-line oxygen sensor (PAROX 1200 H, MBE AG). Subsequently, GC data acquisition was conducted. From the resulting chromatograms, conversion, yield and selectivity towards methacrolein and by-products, especially CO and CO_2, could be calculated (**see SI section 2.2**).

2.4 *Operando* characterization of the catalysts

The catalysts were further characterised by *operando* synchrotron-based XAS, XRD and laboratory-based Raman spectroscopy in a fixed-bed microreactor setup.[37] For each study, the transmission adjusted and thus diluted (XAS) and undiluted catalyst (XRD, Raman spectroscopy) with a sieve fraction of 100-200 µm was filled into a quartz capillary (Ø = 1 mm, 10 µm wall thickness, WJM-Glas Müller GmbH). In each case, the same gas mixture (reaction conditions: $He/O_2/C_4H_8/H_2O$ = 70/14/8/8 vol%; total flow 10 mL/ min) and temperature program (100–600 °C, 2 °C/min) was applied. Prior to the experiments, the temperature inside the capillary was calibrated and the individual heating efficiency of the gas blower (LE MINI SENSOR KIT, Leister Technologies) was considered. Hence, temperatures given refer to the calibrated value inside the capillary, which was measured by an inserted type K thermocouple, and in the case of XRD by the thermal lattice expansion of a silver reference. Controlled dosing of isobutene (N25, Air Liquide), oxygen (N48, Air Liquide) and helium (N50, Air Liquide) was achieved by mass flow controllers (Bronkhorst) with water vapor dosed through a self-built heated steel saturator. Gas lines were heated to 200 °C to prevent water and product condensation. An on-line mass spectrometer (OMNI Star GSD 320, Pfeiffer Vacuum) was used to analyse the product gas mixture and for simplification, solely the unique fragments of each species detected are shown in the mass spectra.

Operando XRD experiments were performed at the Swiss-Norwegian beamline (SNBL) BM01 (ESRF, Grenoble, France). XRD patterns were acquired with the PILATUS@ SNBL diffractometer,[38] including a Pilatus 2M detector (Dectris) and monochromatic beam (λ = 0.63988 Å, 300x300 μm^2). Azimuthal integration of the acquired 2D images was done with Bubble software.[38] For the temperature-programmed measurements, about 7 mg of undiluted catalyst were filled in a quartz glass capillary and XRD patterns were recorded in the middle of

the catalyst bed with 30 s acquisition time. Additionally, a LaB_6 reference was measured for sample to detector distance calibration and to retrieve an instrumental profile function. Sequential Rietveld refinement (2θ = 2.5-27.5°) was performed using TOPAS (v.6, Bruker AXS),[39] with references available in the Inorganic Crystal Structure Database (ICSD, **see SI section 3.1, Table S4**). From Rietveld refinement *e.g.,* crystalline phase amounts were obtained. More details on the sequential Rietveld refinement can be found in the **SI section 3.2**.

Operando Raman spectroscopy was performed with an inVia Raman spectrometer (Renishaw) equipped with a frequency doubled Nd:YAG laser (532 nm, ~100 mW at the source). The laser beam ($Ø_{laser\ spot}$ = ~70 µm) was focused on the capillary with a fibre optics probe (Renishaw) including a long working distance objective. Raman spectra of the undiluted catalysts were recorded with 50% laser intensity, 120 s acquisition time and 2400 lines/mm grating resulting in a spectral range of 60-1320 cm^{-1}. To avoid detecting potential local heterogeneities of the Bi-Mo-Co-Fe-oxides with different sensitivities of the individual metal oxide phases, the Raman optics was moved to detect the metal oxide phases present on average. For that purpose, the Raman optics was mounted on an automated xy-stage and moved periodically (1 period/min) and parallel to the capillary centre (+/- 0.3 mm). This produced averaged spectra representing the whole sample rather than individual heterogeneous regions. Data treatment including cosmic ray removal, noise filtering, truncation and baseline subtraction was performed with WiRE 4.4 (Renishaw). Assignment of Raman bands was carried out based on the metal oxide phases and corresponding references listed in **Table S5 (SI)**.

Operando XAS experiments at Mo K-, Bi L_3-, Co K- and Fe K-edges in transmission mode were performed at ROCK beamline (SOLEIL, Saint-Aubin, France). The unique infrastructure available at ROCK enables fast edge changing,[40-41] and thus the acquisition of all absorption edges during a

single run based on alternate use of two monochromators. The Si(220) monochromator was used for data acquisition at Mo K-edge, for the Bi L_3-, Co K-, and Fe K-edges a Si(111) monochromator (**see SI section 3.3**). Due to their high X-ray absorption, the catalysts were diluted with α-Al_2O_3 in a ratio of 1:4 (m/m), ground, pressed, granulated, and sieved to the desired fraction and ~7 mg of the diluted catalyst was placed in a quartz glass capillary. Subsequently, the capillary was heated and XAS data was acquired in the middle of the catalyst bed at 2 Hz. To acquire data for all metals in a single experiment, a loop in the sequence of Mo K-, Bi L_3- and Fe K-/Co K-edge (recorded in a single scan) was performed. One complete acquisition loop during heating lasted around 6 minutes, with 25 s acquisition at Mo K-, 60 s at Bi L_3- and 180 s at Fe K/Co K-edges. XAS spectra of the initial and final state of the catalysts (before and after heating) were recorded under He atmosphere at 100 °C. At constant temperature, acquisition at Mo K-edge lasted 300 s, whereas at Bi L_3- and Fe K-/Co K-edges it lasted 600 s each. The spectra of one acquisition period were averaged to produce a single spectrum for each edge. Energy calibration, averaging, background subtraction, and normalization were conducted with the beamline software.[42] Further data treatment was performed with the software package IFEFFIT.[43] More details on XAS data acquisition and analysis are given in the **SI section 3.3**.

3 Results and Discussion

3.1 Laboratory-based *ex situ* characterization and catalytic performance

Three Bi-Mo-Co-Fe-O catalysts with different metal ratios were synthesized by FSP (**Table 1**) and calcined at 500 °C for 5 h under static air. ICP-OES results showed good agreement between targeted and experimentally verified metal compositions (**see SI section 1.1**), indicating its precise control *via* FSP. No compositional changes were observed before and after catalytic testing for

several days on stream (up to 5 days), demonstrating a high stability of the catalysts under the applied condition (*e.g.*, no loss of molybdenum as observed in ref. [44-45]). According to electron microscopy results (SEM-EDX**, see SI section 1.2**) and Raman mapping, FSP gave direct access to homogeneously distributed metal oxide nanoparticles on the µm level, which remained evenly distributed after catalytic testing.

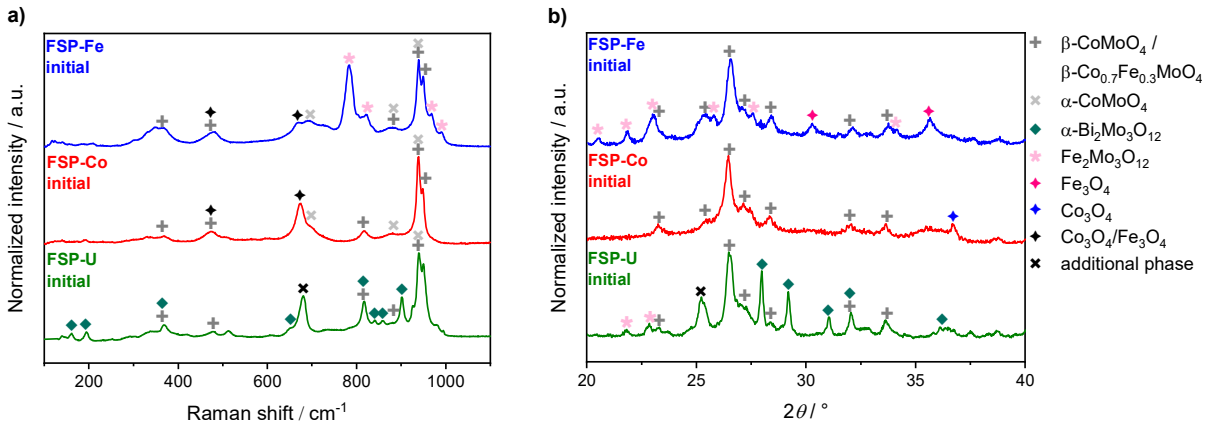

Figure 1. *Ex situ* Raman spectra (a) and XRD patterns (b, lab source, Cu K_α radiation) of the initial (calcined at 500 °C) states of flame spray prepared samples FSP-U, FSP-Co and FSP-Fe.

As a consequence of varying catalyst composition, significant changes in the metal oxide phases present were identified by Raman spectroscopy (**Fig. 1a**) and laboratory XRD (**Fig. 1b**). All three catalysts exhibited characteristic features assigned to β-$CoMoO_4$ / β-$Co_{0.7}Fe_{0.3}MoO_4$ and α-$CoMoO_4$. XRD revealed the additional presence of $Fe_2Mo_3O_{12}$ in FSP-Fe and FSP-U, while α-$Bi_2Mo_3O_{12}$ was only detected in FSP-U. Crystalline Fe_3O_4 and Co_3O_4 were solely detected in FSP-Fe and FSP-Co, respectively. Both spinel-type oxides were also observed by Raman spectroscopy, but corresponding mixed metal oxide spinels can in this case not be excluded due to similar band positions.[46-48] Moreover, a reflection (2θ = 25.2°, λ = 1.5406 Å) was found in the XRD pattern of FSP-U which could not be assigned to a metal oxide phase referenced in the ICSD (**see SI Table S4**) and is therefore labelled as "additional" phase (**see SI section 1.3**).

The catalytic performance of FSP-Co, FSP-Fe and FSP-U during selective isobutene oxidation was tested in a lab-scale fixed-bed reactor (**see SI section 2.1**). The corresponding results of each catalyst tested with SiC dilution (1:5) are shown in **Figure 2**. The samples already differed in their catalytic activity as indicated by different oven temperatures required for the start of the selective oxidation process. While FSP-Co and FSP-Fe became active at 420 °C and 400 °C, a significantly higher temperature (490 °C) was needed for FSP-U. This ignition of FSP-Co and FSP-Fe at lower temperatures was also found for tests without catalyst dilution (**see SI section 2.3**). In this case, the high isobutene conversions for FSP-Co and FSP-Fe (~ 75-80 %) additionally resulted in almost full oxygen consumption (~ 95-99 %) with high heat release, while it was found lower for FSP-U (~ 80 %) at similar conversion. Additionally, carbonaceous deposits were observed in all three samples after catalytic testing (**see SI section 6**). Still, the trends in catalytic activity and selectivity and thus methacrolein yields were only partly affected by dilution.

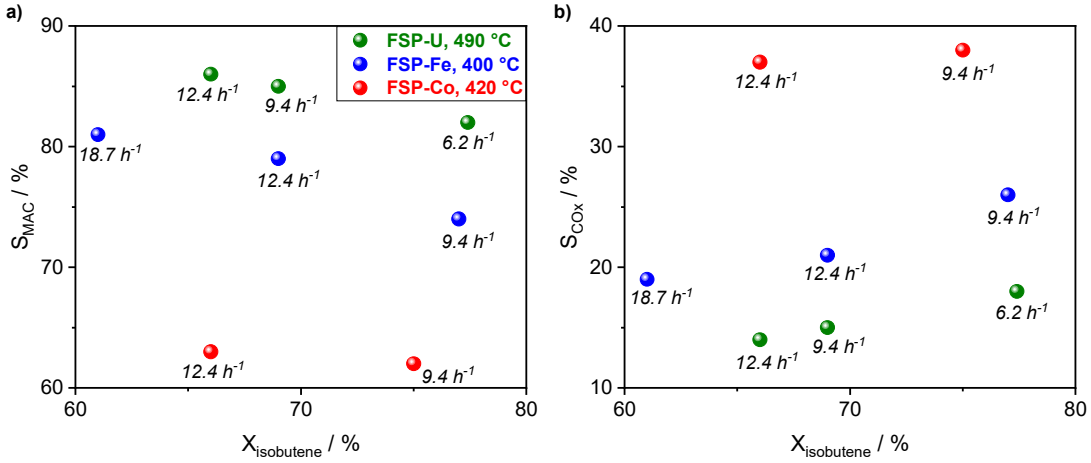

Figure 2. Methacrolein selectivity (a) and CO_x selectivity (b) over isobutene conversion of FSP-Co, FSP-Fe and FSP-U measured at corresponding activation temperatures (400, 420 and 490 °C) in a lab-scale testing unit ($N_2/O_2/C_4H_8/H_2O$ = 70/14/8/8 vol%) at different WHSVs (6.2-18.7 h^{-1}). All catalysts were diluted with SiC (1:5).

In general, FSP-U performed best with respect to high isobutene conversion and methacrolein selectivity (66 % and 86 % at WHSV = 12.4 h^{-1}, respectively). This corresponds to a reaction rate of $172 \cdot 10^{-6}$ $g_{MAC}/(g_{cat} \cdot h)$. FSP-Fe showed a slightly higher conversion (69 % at 12.4 h^{-1}), but a lower methacrolein selectivity (79 % at 12.4 h^{-1}) than FSP-U, and thus a reaction rate of $169 \cdot 10^{-6}$ $g_{MAC}/(g_{cat} \cdot h)$. In contrast, FSP-Co showed a lower selectivity due to high presence of the total oxidation products CO and CO_2 (37 % at 12.4 h^{-1}) and the lowest isobutene conversion (66 % at 12.4 h^{-1}), which corresponds to a reaction rate of $119 \cdot 10^{-6}$ $g_{MAC}/(g_{cat} \cdot h)$. Other minor by-products were detected for all three catalysts but their sum was very small (selectivity ~ 2%).

Notably, isobutene conversions were in a similar regime for all three catalysts (~ 60-70 % at 12.4 h^{-1}) and similar values could also be achieved for FSP-U at lower temperatures (< 490 °C) by using less diluent or a higher catalyst mass. In other words, same catalyst masses with same catalyst dilution were chosen for comparability of the catalytic tests, but strong dilution was only necessary for FSP-Fe and FSP-Co due to high activity and heat release. In contrast, the activity of FSP-U was more moderate and controllable. This trend was not only observed in the herein presented lab-scale testing unit, but also for the significantly smaller scale in a microcapillary reactor (**see section 3.2**). Consequently, these results emphasize that the variations in catalytic performance are related to the variations in metal oxide phase composition of each catalyst, their phase amounts and/ or surface area. Such variations were induced by different initial metal ratios of FSP-Co, FSP-Fe and FSP-U (**Fig. 3**). According to the above described *ex situ* characterization, the catalysts containing less than 50 mol% Mo (FSP-Co, FSP-Fe) tended to form (crystalline) single metal oxide phases with higher surface areas (**Table 1**) prior to catalytic testing, which may explain their high activity. However, surface areas of all three catalysts decreased upon time on stream (to comparable values) while catalytic performance remained constant, emphasizing a less important role during

operation. Hence, the metal oxide phases present under operating conditions probably have a more predominant influence than the surface area. This was supported by previous studies in selective propylene oxidation over Bi-Mo-Co-Fe-oxides.[24, 27] As phase formation is strongly dependent on the temperature and gas phase conditions,[5, 26, 49] it is crucial to investigate the catalysts under reaction conditions and therefore complementary *operando* characterization was performed.

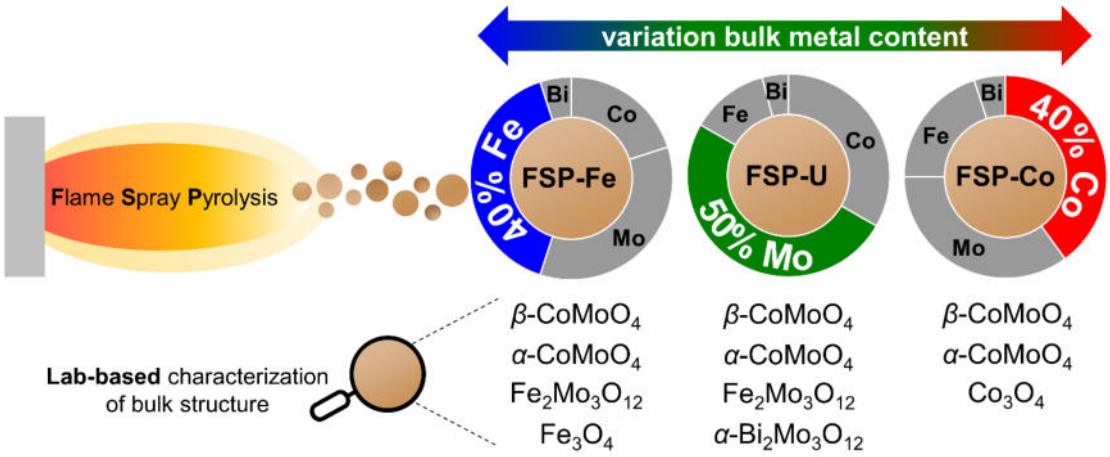

Figure 3. Illustration of the catalyst compositions of FSP-Fe, FSP-U and FSP-Co, their preparation by flame spray pyrolysis and the corresponding main metal oxide phases detected after synthesis and calcination at 500 °C using laboratory-based XRD and Raman spectroscopy.

3.2 *Operando* characterization by synchrotron XRD, XAS and Raman spectroscopy

In order to monitor the metal oxide phase evolution of FSP-Co, FSP-Fe and FSP-U during temperature-programmed reaction (TPRxn, selective oxidation of isobutene), complementary *operando* synchrotron XRD, Raman spectroscopy and multi-edge XANES and EXAFS studies in the QEXAFS mode were performed. While Raman spectroscopy provided information on the amorphous and crystalline phases of the bulk material, synchrotron XRD in combination with Rietveld refinement gave additional and precise insights in terms of crystalline metal oxide phase

composition and their amounts. XAS at Mo K-, Bi L_3-, Co K- and Fe K-edges allowed to monitor structural changes of each of the four metals independently and almost simultaneously.

The amounts of crystalline phases of the three initial catalysts obtained by Rietveld refinement prior to catalytic tests at 100 °C are summarized in **Table 2**. Like for the *ex situ* results of the initial catalysts at room temperature (**Fig. 1a, b**), β-$CoMoO_4$/ β-$Co_{0.7}Fe_{0.3}MoO_4$ was detected in each catalyst. Due to the isostructural nature of both metal oxides, a clear differentiation was not possible by XRD and thus Rietveld refinement was only performed with the β-$Co_{0.7}Fe_{0.3}MoO_4$ structure as in ref. [27] (further details, **see SI section 4**). Still, formation of β-$Co_{0.7}Fe_{0.3}MoO_4$ appeared favourable at higher temperatures and therefore will be discussed in the following for each catalyst together with additional, complementary methods.

Table 2. Overview of crystalline phases and phase fractions of FSP-Co, FSP-Fe and FSP-U as determined by synchrotron XRD with Rietveld refinement before catalytic testing.

Crystalline phases *via* synchrotron XRD	**Phase composition *via* Rietveld refinement / wt%**		
	FSP-Co	**FSP-Fe**	**FSP-U***
β-$Co_{0.7}Fe_{0.3}MoO_4$	37.3 ± 0.3	37.6 ± 0.3	58.6 ± 0.8
α-$CoMoO_4$	30.5 ± 0.3	9.9 ± 0.3	12.9 ± 0.6
$Fe_2Mo_3O_{12}$	-	21.5 ± 0.3	12.0 ± 0.8
α-$Bi_2Mo_3O_{12}$	-	-	16.5 ± 0.4
$Bi_3FeMo_2O_{12}$	6.0 ± 1.3	3.2 ± 1.0	-
Fe_3O_4	19.0 ± 0.6	27.8 ± 0.3	-
Co_3O_4	6.9 ± 0.3	-	-

*additional phase detected (see **SI section 4.3**), absolute phase fractions in FSP-U only represent a trend.

Overall, FSP-U initially contained a significant higher fraction of crystalline β-$CoMoO_4$/ β-$Co_{0.7}Fe_{0.3}MoO_4$ (~ 59 wt%) compared to FSP-Co (~ 38 wt%) and FSP-Fe (~ 37 wt%). However, as one pronounced peak (10.35° 2θ, λ = 0.63988 Å) prior to ignition of the reaction could not be

assigned to a metal oxide phase (**see SI section 4.3**), the absolute phase composition detected *via* XRD for FSP-U only represents a trend. Still, the *ex situ* Raman spectra of the initial catalyst states (**Fig. 1a**) indicated a higher amount of β-$CoMoO_4$ in FSP-U by the more pronounced shoulder at ~ 949 cm^{-1}.[50-51] In contrast, a higher amount of crystalline α-$CoMoO_4$ was detected by synchrotron XRD in FSP-Co (~ 30 wt%), compared to FSP-Fe (~ 10 wt%) and FSP-U (~ 13 wt%). Moreover, crystalline Fe_3O_4 was only detected in FSP-Co and FSP-Fe. Other crystalline phases detected in specific initial catalyst states included Co_3O_4 in FSP-Co, $Bi_3FeMo_2O_{12}$ in FSP-Co and FSP-Fe, $Fe_2Mo_3O_{12}$ in FSP-Fe and FSP-U, as well as α-$Bi_2Mo_3O_{12}$ solely detected in FSP-U. These results are supported by complementary *operando* Raman spectroscopy (**Fig. 4**) and multi-edge XAS results (**see SI section 5**) which are more sensitive to amorphous phases.

A direct comparison of the *operando* synchrotron XRD data (**Fig. 4a-c**) with simultaneously acquired mass spectrometric (MS) data (**Fig. 4d-f**) and complementary Raman spectroscopy results (**Fig. 4g-i**) for all three catalysts during TPRxn is presented in **Figure 4**. Based on catalytic activity data over α-Al_2O_3, the contribution of homogeneous gas phase reactions was found negligible especially below 500 °C compared to catalytic reaction (**see ESI section 7**). In general, all crystalline metal oxide phases were stable during heating up to the start of the reaction, most likely due to the catalyst pre-treatment conditions (calcination at 500 °C, 5 h). Moreover, the trends concerning ignition temperature and oxygen conversion of all three catalysts measured in the microcapillary setup were in line with the results obtained in the lab-scale testing unit (**see section 3.1**), *i.e.* FSP-Co and FSP-Fe ignited at lower temperatures (~ 395 °C and 380 °C, respectively) than FSP-U (~ 420 °C). In addition, a strong decrease of the MS signal of m/z = 32 for FSP-Co and FSP-Fe (**Fig. 4d, e**) confirmed a high oxygen consumption (~ 99%) for these two catalysts. The differences in absolute ignition temperatures measured in the microreactor and lab-scale

testing unit were most likely attributed to the different WHSV and catalyst dilution in both setups. Since all three FSP-prepared catalysts were investigated under identical reaction conditions and showed a similar behaviour in the two different reactor types (microreactor and lab-scale testing unit) these results strongly suggest a predominant effect of the (initial) metal oxide phase composition on catalytic activity. Therefore, the corresponding phase transformations of each catalyst will be discussed in the following **sections 3.2.1** and **3.2.2**.

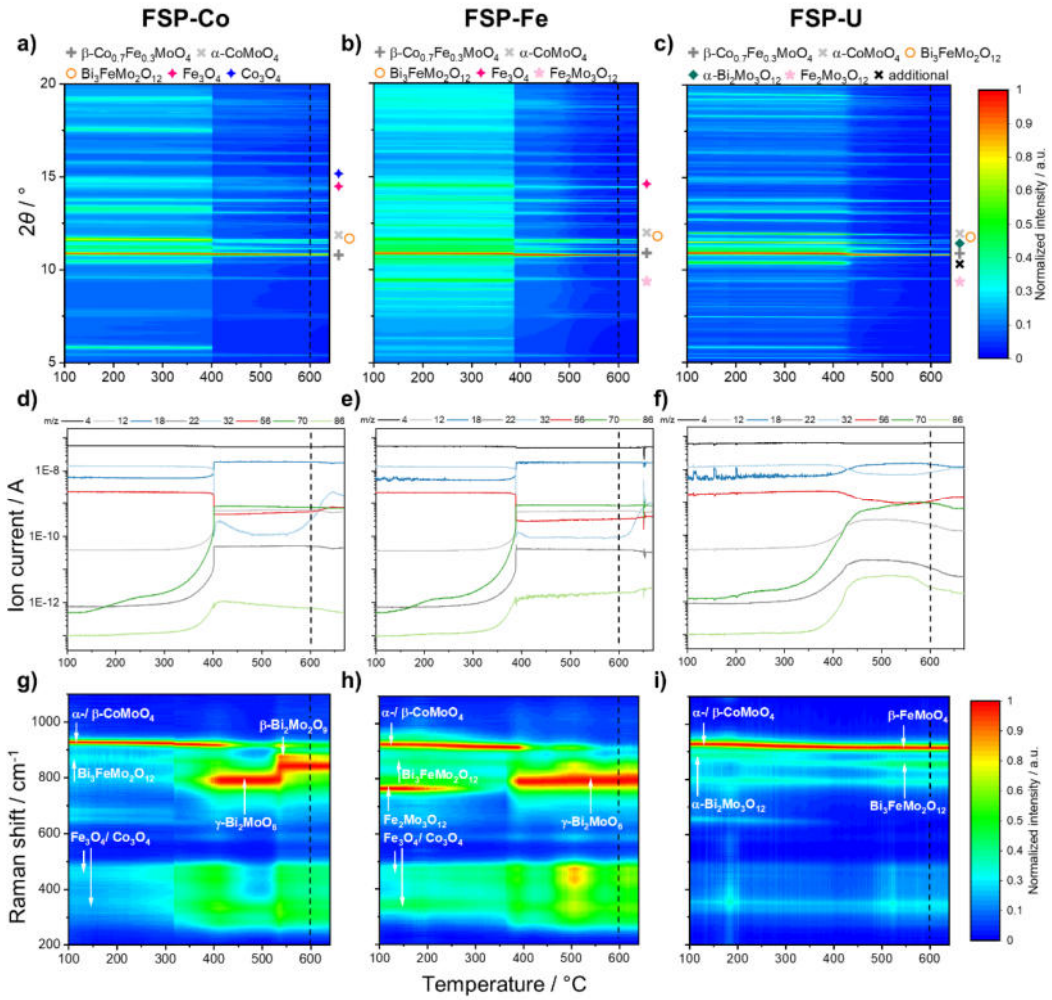

Figure 4: Normalized 2D XRD patterns (a-c), simultaneously measured MS data (d-f) and normalized 2D Raman intensity plots (g-i) of FSP-Co (left), FSP-Fe (middle) and FSP-U (right)

with the assignment of metal oxide phases measured during TPRxn (100-600 °C, 2 °C/min, $He/O_2/C_4H_8/H_2O$ = 70/14/8/8 vol%). Dotted vertical lines indicate the start of the isothermal period at 600 °C (15 min). In (a-c), only the main reflections of the present phases are labelled.

3.2.1 Phase transformations in FSP-U

During catalytic reaction several pronounced structural changes occurred in all three catalysts, as exemplarily shown by the XRD patterns and Raman spectra of FSP-U acquired under reaction conditions at 100 °C and 600 °C (**Fig. 5**).

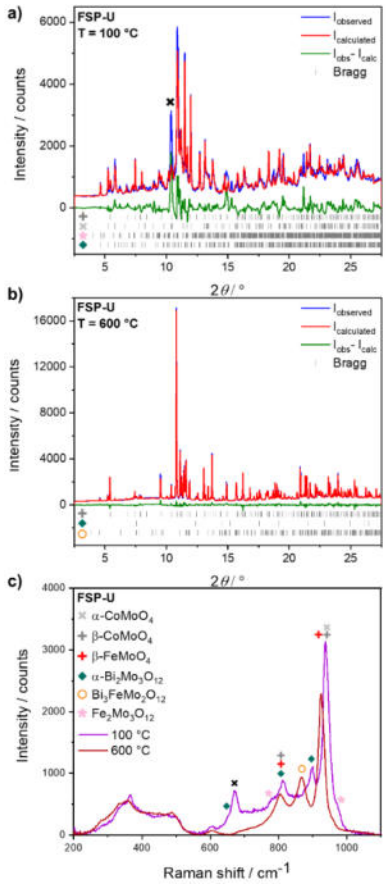

Figure 5. Selected synchrotron XRD pattern with corresponding Rietveld refinement fit of FSP-U acquired in reaction atmosphere ($He/O_2/C_4H_8/H_2O$ = 70/14/8/8 vol%) at 100 °C (a) and 600 °C (b) and complementary acquired Raman spectra (c). Label (✖) in (a) refers to main reflection of the "additional phase".

For FSP-U, *operando* XRD with Rietveld refinement unravelled the disappearance of $Fe_2Mo_3O_{12}$, α-$CoMoO_4$ and the "additional phase" (~ 420 °C, **Fig. 6**). While also the fraction of crystalline α-$Bi_2Mo_3O_{12}$ slightly decreased in the temperature range of around 420-560 °C (~ 16 wt% to 12 wt%), a significant increase of crystalline β-$CoMoO_4$/ β-$Co_{0.7}Fe_{0.3}MoO_4$ was detected (~ 69 wt% to 86 wt%).

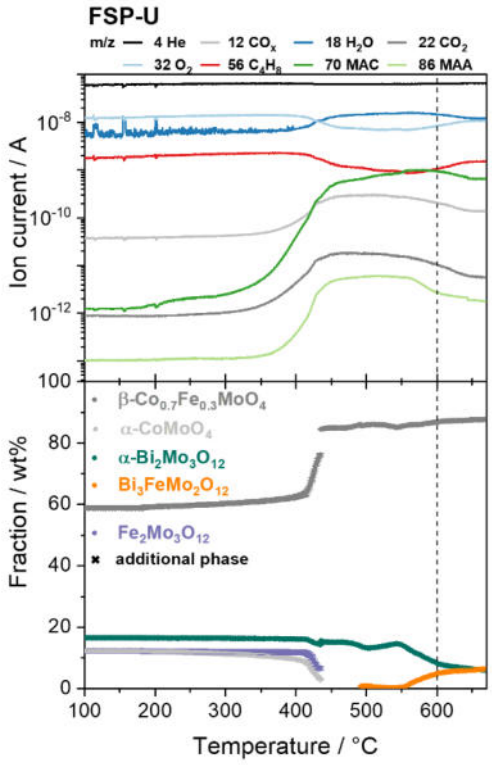

Figure 6. MS data (top) and evolvement of crystalline phases (bottom) derived from synchrotron XRD with Rietveld refinement of FSP-U measured during temperature-programmed reaction (100-600 °C, 2 °C/min, $He/O_2/C_4H_8/H_2O$ = 70/14/8/8 vol%). Dotted vertical lines indicate the start of the isothermal period at 600 °C (15 min). An additional phase in the XRD patterns of FSP-U was detected before ignition of the reaction (< 420 °C).

At temperatures > 560 °C, the formation of crystalline $Bi_3FeMo_2O_{12}$ was observed, involving a further decrease of the α-$Bi_2Mo_3O_{12}$ amount to ~ 8 wt% by reaching 600 °C. The Raman spectra

(**Fig. 5c**) further indicated the formation of β-$FeMoO_4$ upon ignition, due to a shift in the main band from ~ 936 to 924 cm^{-1}.[52-53] Moreover, β-$Co_{0.7}Fe_{0.3}MoO_4$ was likely formed during heating, as also the insertion of Fe into the β-$CoMoO_4$ structure is associated with a shift of its band towards lower wavenumbers.[53] Additionally, the XANES spectra at Co K-edge (**see SI section 5.3**) showed the presence of a mixture of α-/β-$CoMoO_4$ in the initial catalyst state, that transformed to a structure closer to β-$CoMoO_4$ as a distinct feature at ~ 7732 eV corresponding to α-$CoMoO_4$ became less pronounced during heating.[54] LCF of XANES spectra at Fe K-edge further indicated a reduction of Fe^{3+} to Fe^{2+}, with the final spectrum being close to $FeMoO_4$ (**Fig. 7**).[55] Thus, these complementary results suggest that a reduction of iron molybdate took place according to **Eq. (1)** in FSP-U.

$$Fe_2Mo_3O_{12} \rightarrow 2\ FeMoO_4 + MoO_3 + [O] \quad \textbf{(1)}$$

In this case, no MoO_3 was detected by XRD, XAS or Raman spectroscopy, probably due to fast incorporation of Fe^{2+} into β-$CoMoO_4$, forming β-$Co_{0.7}Fe_{0.3}MoO_4$ as schematically given in **Eq. (2)**.[27]

$$CoMoO_4 + MoO_3 + Fe_xO_y \rightarrow Co_{0.7}Fe_{0.3}MoO_4 \quad \textbf{(2)}$$

Additionally, $Bi_3FeMo_2O_{12}$ formation during reaction was confirmed by LCF results (XANES at Mo K- and Bi L_3-edges) and is most likely induced by the incorporation of Fe^{3+} into α-$Bi_2Mo_3O_{12}$. Since LCF at Fe K-edge confirmed the Fe^{3+} reduction, this opposite trend might be explained by the rather low amount of $Bi_3FeMo_2O_{12}$ detected.[27] While XRD showed the formation of crystalline $Bi_3FeMo_2O_{12}$ above 560 °C, amorphous $Bi_3FeMo_2O_{12}$ was already found by Raman spectroscopy at lower temperatures (> 500 °C) (**Fig. 4i**). At the same time, the on-line MS data showed an increase in methacrolein (signal for m/z 70) and a decrease in isobutene (m/z 56) at the onset of the reaction (420-530 °C). Simultaneously, CO_x (m/z = 12 and 22) remained constant,

indicating an increase in methacrolein selectivity. Furthermore, methacrolein selectivity increased at nearly constant isobutene conversion in the temperature regime from ~ 530-585 °C. This indicates a crucial role of the $Bi_3FeMo_2O_{12}$ phase for methacrolein selectivity. At temperatures above 585 °C, a decrease of isobutene conversion was detected, accompanied by a decrease of intensities for m/z = 12, 22 and 70 with similar slopes. This might be due to full incorporation of Fe^{3+} into α-$Bi_2Mo_3O_{12}$ and its reduction to Fe^{2+} with incorporation into ternary β-$Co_{0.7}Fe_{0.3}MoO_4$.

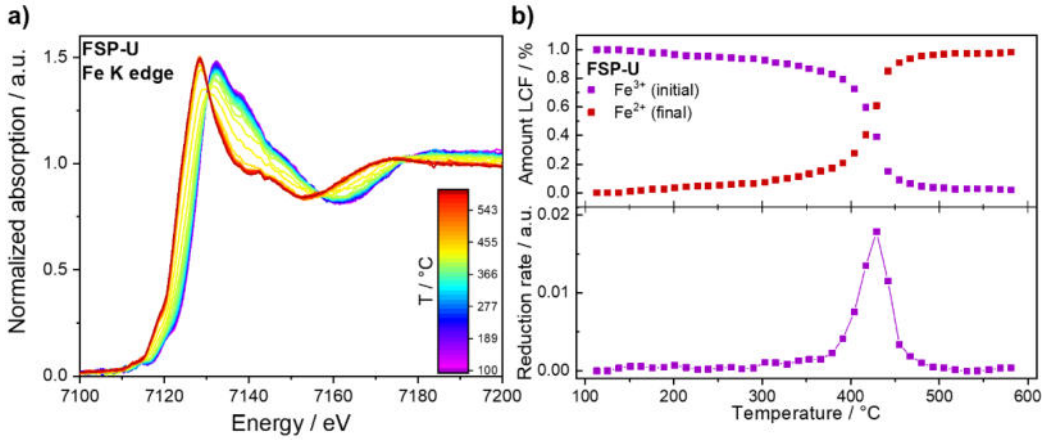

Figure 7. Series of normalized *operando* Fe K-edge XANES spectra of FSP-U (a) acquired during TPRxn (100-600 °C, $He/O_2/C_4H_8/H_2O$ = 70/14/8/8 vol%) with LCF results (b, top) using first and last spectrum and corresponding iron reduction rates (b, bottom).

The phase transformations observed for FSP-U during temperature-programmed isobutene oxidation are similar to those observed by Stehle *et al.* during selective oxidation of propylene.[27] However, in that study, no catalyst pre-treatment (*i.e.*, calcination) was performed before the experiments, thus revealing the interim formation of MoO_3 during temperature-programmed propylene oxidation as observed here during calcination (**see SI section 1.3**). Additionally, the detection of MoO_3 might also be directly correlated to the reaction rate in the respective selective olefin oxidation, which seems to be enhanced by the additional methyl group present in isobutene. This is for example reflected by the reduction rate of Fe^{3+} during isobutene reaction, which was

significantly higher compared to the iron reduction rate found during propylene oxidation. However, the onset of the reaction was shifted to higher temperatures ($\Delta T = \sim 70$ °C) in the case of isobutene. This observation might be due to the catalyst pre-treatment (calcination), but is probably mainly caused by the different properties of the hydrocarbon reactants (*e.g.*, different structures). According to that, structural transformations seem to generally proceed faster in the selective oxidation of isobutene but were found to require higher temperatures in the case of FSP-U compared to the microreactor studies in propylene oxidation.

3.2.2 Phase transformations in FSP-Fe and FSP-Co

Similar to FSP-U, the structural changes detected in FSP-Fe included the decomposition of $Fe_2Mo_3O_{12}$ to $FeMoO_4$ (see **Eq. (1)**) at reaction onset (~ 380 °C), as shown by *operando* XRD (**Fig. 8a**).

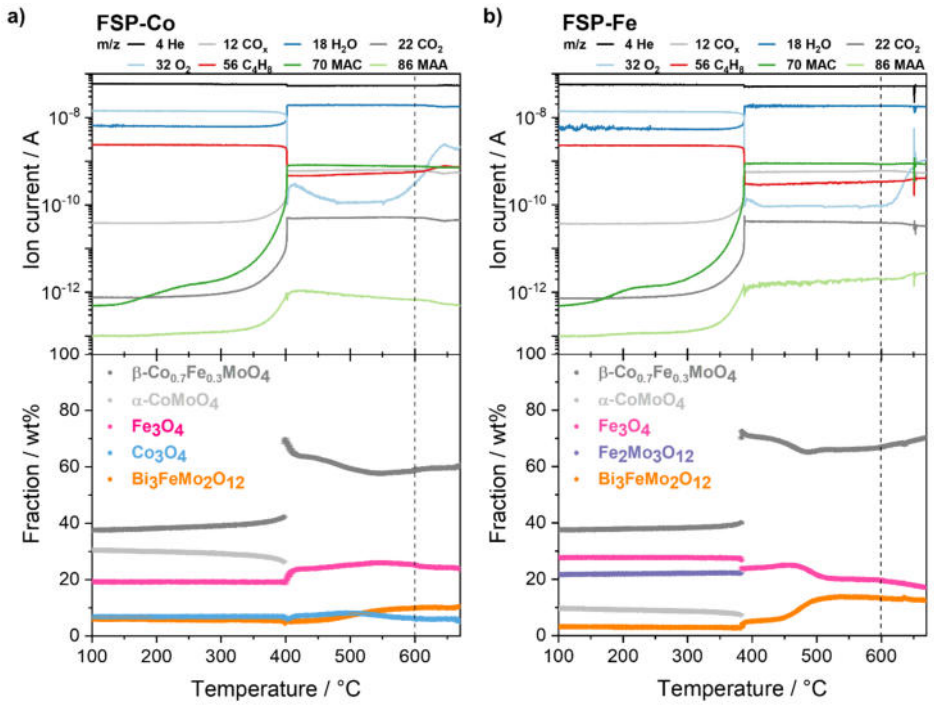

Figure 8. MS data (top) and evolvement of crystalline phases (bottom) derived from synchrotron XRD with Rietveld refinement of FSP-Fe (a) and FSP-Co (b) measured during temperature-

programmed reaction (100-600 °C, 2 °C/min, He/O_2/C_4H_8/H_2O = 70/14/8/8 vol%). Dotted vertical lines indicate the start of the isothermal period at 600 °C (15 min).

Additionally, Raman spectroscopy (**Fig. 9a**) indicated a reduction of $Fe_2Mo_3O_{12}$ at lower temperatures (~ 230 °C) compared to the phase transformations observed by XRD. This suggests that structural changes in terms of short-range order occurred already prior to the *in situ* formation of the active catalyst. Despite the initially higher amount of $Fe_2Mo_3O_{12}$ in FSP-Fe (~ 22 wt%) compared to FSP-U (~ 12 wt%), no MoO_3 formation was observed *via* XRD nor Raman spectroscopy. Consequently, the fast incorporation of MoO_3 with formation of β-$Co_{0.7}Fe_{0.3}MoO_4$ (see **Eq. (2)**) occurred also in the case of FSP-Fe which is supported by the shift towards lower wavenumbers in the Raman spectra at higher temperatures, which also remained shifted after cooling down. Moreover, Raman spectroscopy revealed the formation of amorphous γ-Bi_2MoO_6 at ~ 380 °C, which was stable up to 600 °C.

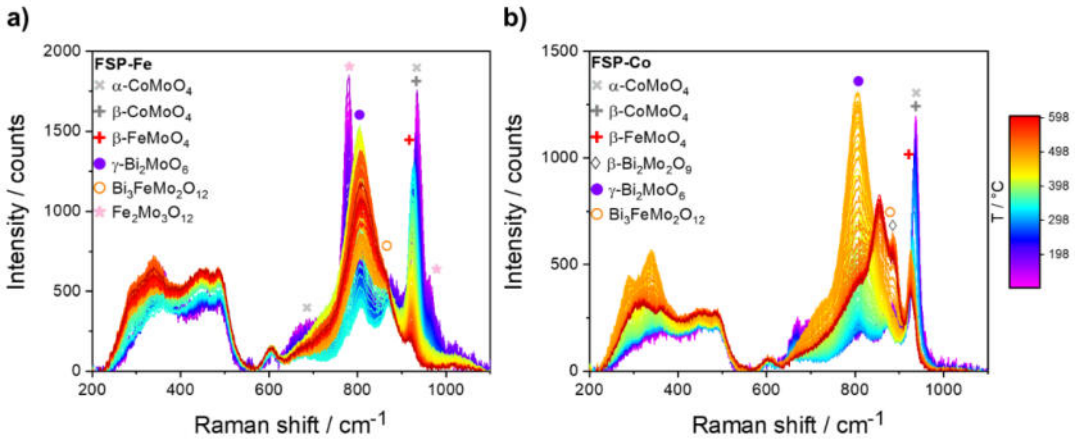

Figure 9. Overlaid Raman spectra (non-normalized) of FSP-Fe (a) and FSP-Co (b) acquired during TPRxn.

Notably, the characteristic bands for γ-Bi_2MoO_6 (718, 799, 845 cm^{-1})[15, 56] are rather broad and might overlap with other metal oxide bands. However, according Kongmark *et al.* γ-Bi_2MoO_6 is

suggested to be formed from $[Bi_2O_2]^{2+}$ and tetrahedral $[MoO_4]^{2-}$ species.[56-57] Such tetrahedral $[MoO_4]^{2-}$ species are e.g. present in β-$CoMoO_4$,[54, 58] β-$FeMoO_4$[59] and Bi_3FeMoO_{12}[60]. Since amorphous γ-Bi_2MoO_6 appeared simultaneously to the transformation of crystalline α-$CoMoO_4$ to β-$CoMoO_4$ (**Fig. 8a**), indicating that octahedrally coordinated Mo^{6+} ions were fully transformed into tetrahedrally coordinated Mo^{6+} within the cobalt molybdate structure, this structural change might be correlated to the γ-Bi_2MoO_6 formation process. Such a transformation from crystalline α-$CoMoO_4$ to β-$CoMoO_4$ was also observed for FSP-Co upon catalyst activation around 395 °C (**Fig. 8b**) with simultaneous formation of amorphous γ-Bi_2MoO_6 (**Fig. 9b**). Moreover, LCF of the XANES spectra at the Bi L_3-edge showed a contribution of Bi_2O_3 only in the case of FSP-Co and FSP-Fe (**see SI section 5.1 and 5.2**), thus supporting the assumed γ-Bi_2MoO_6 formation process.

Compared to FSP-U, the *in situ* activation of both FSP-Co and FSP-Fe was accompanied by faster structural transformations (< 30 s, as seen by *operando* XRD) and a rapid increase of isobutene and oxygen conversion (**Fig. 4**). Remarkably, the catalytic performance of FSP-Co and FSP-Fe remained nearly constant from ignition up to 600 °C, while FSP-U showed a more pronounced decrease in isobutene conversion and thus product formation above 585 °C. However, in particular oxygen consumption slightly decreased from ~ 99 to 89 % for FSP-Co above ~550 °C and for FSP-Fe while holding at 600 °C. Simultaneously, the product concentration of CO_x slightly decreased and methacrolein formation remained constant in both cases, while for FSP-Fe even methacrylic acid formation slightly increased. These changes in selectivity at high temperatures were accompanied by structural changes. In the case of FSP-Co, the decrease of oxygen consumption was accompanied by a shift of the most intense Raman band corresponding to γ-Bi_2MoO_6 from ~ 803 cm^{-1} to ~ 854 cm^{-1} and 886 cm^{-1}, indicating the presence of β-$Bi_2Mo_2O_9$ (886 cm^{-1})[61] above 540 °C. The band at 854 cm^{-1} could not be unambiguously assigned to any

particular phase. The position is located between the characteristic Mo-O stretching bands of γ-Bi_2MoO_6 (MoO_6 octahedra) and scheelite-structured $Bi_3FeMo_2O_{12}$ and β-$Bi_2Mo_2O_9$ (MoO_4 tetrahedra) indicating that a change in the Mo-O bond lengths might have taken place at high temperatures. Thus, the high oxygen consumption could be related to γ-Bi_2MoO_6 formation upon ignition, as the aurivillius-type γ-Bi_2MoO_6 exhibits octahedral coordination of Mo^{6+} and is ascribed to provide fast oxygen transport through the lattice.[19, 62] In contrast, scheelite-structured β-$Bi_2Mo_2O_9$ and $Bi_3FeMo_2O_{12}$ contain tetrahedrally coordinated Mo^{6+}, that is claimed to provide a high number of active sites for hydrogen abstraction during reaction.[63]

Compared to FSP-Co, *operando* Raman measurements of FSP-Fe did not reveal such a pronounced shift of the γ-Bi_2MoO_6 Raman band. As the corresponding decrease of oxygen consumption was observed in FSP-Fe during holding time at 600 °C, such a transformation may have been shifted to higher temperatures and longer time on stream due to a higher amount of amorphous γ-Bi_2MoO_6. This may be due to the higher amount of tetrahedrally coordinated $[MoO_4]^{2-}$ species in the initial catalyst state, as observed by XRD (less α-$CoMoO_4$) and XANES at Mo K-edge (**see SI section 5**). At the same time, a transformation of significantly higher amounts of crystalline α-$CoMoO_4$ (~ 30 wt%) to β-$CoMoO_4$ was observed for FSP-Co after catalyst activation compared to FSP-Fe (~ 10 wt%), implying the formation of more tetrahedrally coordinated $[MoO_4]^{2-}$ species with the start of the reaction. This might in turn result in a higher amount of γ-Bi_2MoO_6 in FSP-Co. However, γ-Bi_2MoO_6 formation includes $[MoO_4]^{2-}$ species, but also their interaction with $[Bi_2O_2]^{2+}$ entities.[57] LCF of XANES at Bi L_3-edge revealed similar amounts of Bi_2O_3, $Bi_3FeMo_2O_{12}$ and γ-Bi_2MoO_6 for both FSP-Co and FSP-Fe, thus not evidencing any formation of an increased amount of γ-Bi_2MoO_6 in FSP-Fe compared to FSP-Co. As amorphous γ-Bi_2MoO_6 was detected in the final states (600 °C) of both FSP-Co and FSP-Fe, the

observed shift or difference in band intensity of the γ-Bi_2MoO_6 phase in the Raman spectra of FSP-Co could either be correlated to a local heterogeneity (**see section 2.5**) or to different sensitivities of Raman spectroscopy towards individual metal oxide phases.

Finally, it should be mentioned that a change in catalyst colour was clearly visible towards the end of the catalyst bed of FSP-Co and FSP-Fe. This could indicate a structural gradient along the catalyst bed and additionally explain the decrease of oxygen conversion observed at higher temperatures. Still, the herein discussed active role of γ-Bi_2MoO_6 is in line with activity trends found for 2-component bismuth molybdate catalysts during selective propylene oxidation, where a higher conversion over FSP-prepared γ-Bi_2MoO_6 was observed compared to α-$Bi_2Mo_3O_{12}$.[35] Also Krenzke *et al.* reported on a very high activity of γ-Bi_2MoO_6 that can result in uncontrolled reaction temperature during propylene oxidation.[64] However, the active nature of γ-Bi_2MoO_6 was significantly more pronounced in the herein discussed 4-component systems, probably due to the presence of further metal oxide phases and resulting synergistic effects.

Besides the formation of amorphous γ-Bi_2MoO_6, high amounts of crystalline Fe_3O_4 were found in FSP-Co and FSP-Fe during the entire TPRxn (**Fig. 8**). This was additionally observed by the XANES spectra of FSP-Co at Fe K-edge (**Fig. 10**) that were closest to Fe_3O_4 in the entire temperature regime and thus did not evidence the reduction of Fe^{3+} as it was observed for FSP-U (**Fig. 7**). Since the Fe^{2+}/Fe^{3+} redox couple is also reported to be crucial for a constant supply of lattice oxygen to the active Bi-Mo-O centres,[27, 53] the constantly high activity of FSP-Co and FSP-Fe might additionally be correlated to the constant presence of high amounts of Fe_3O_4 (Fe^{2+}/Fe^{3+}). Hence, we assume that especially the interaction of γ-Bi_2MoO_6 and Fe_3O_4 is responsible for the constantly high isobutene conversion with (too) high oxygen consumption observed up to high temperatures during TPRxn. Since the slight decrease in activity observed for FSP-Fe at ~ 600 °C

was in contrast to FSP-Co not accompanied by a pronounced structural change regarding the amorphous γ-Bi_2MoO_6, but instead showed a slight decrease in crystalline Fe_3O_4 (20 to 17 wt%), this further supports our assumption.

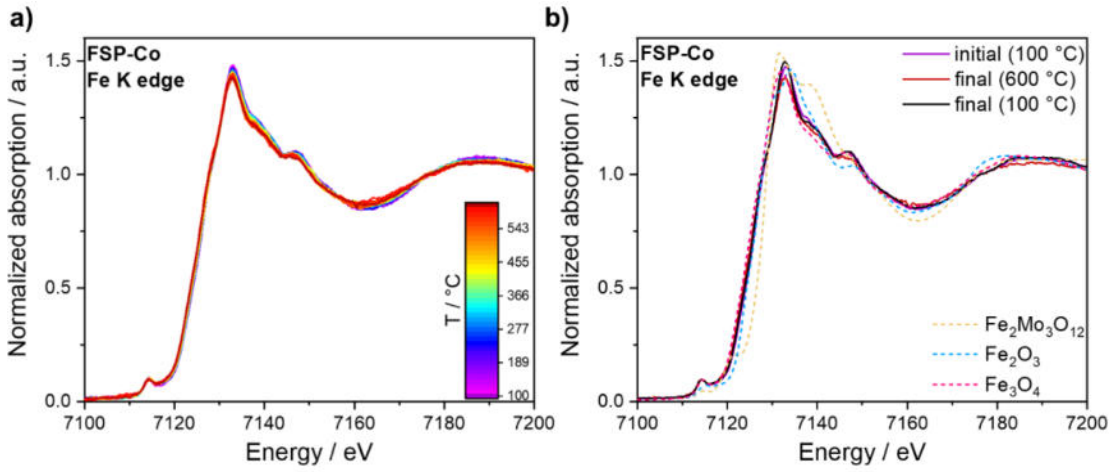

Figure 10. Series of normalized *operando* Fe K-edge XANES spectra of FSP-Co (a) acquired during TPRxn (100-600 °C, $He/O_2/C_4H_8/H_2O$ = 70/14/8/8 vol%) and normalized Fe K-edge XANES spectra for FSP-Co under isothermal conditions (b) with selected references (dotted lines).

At the same time, $Bi_3FeMo_2O_{12}$, which was found to be selective towards methacrolein in FSP-U, was also detected in FSP-Fe and FSP-Co (**Fig. 8**). Remarkably, the amount of crystalline $Bi_3FeMo_2O_{12}$ in FSP-Co increased up to ~ 10 wt% at 600 °C, which was higher than in the selective FSP-U catalyst. Since the phase amount of $Bi_3FeMo_2O_{12}$ was highest in FSP-Fe, while methacrolein selectivity was still lower than in FSP-U, this suggests that the presence of $Bi_3FeMo_2O_{12}$ is not solely responsible for the selectivity. These results underline that in particular phase interactions are crucial for catalytic performance.

In the case of FSP-Co, XANES spectra at the Fe K-edge confirmed the presence of Fe_3O_4 and $Bi_3FeMo_2O_{12}$, but also indicated a minor amount of $Fe_2Mo_3O_{12}$ at the Mo K-edge (**see SI section 5.2**). Thus, the low phase amount of iron molybdate and the consequently higher amount

of pure iron oxides (Fe_2O_3, Fe_3O_4) might have led to reduction of $Fe_2Mo_3O_{12}$ (see Eq. **(1)**) to a lower extent, thus forming less $FeMoO_4$ and MoO_3. Hence, less Fe^{2+} could be incorporated in β-$CoMoO_4$ forming less β-$Co_{0.7}Fe_{0.3}MoO_{12}$ (see Eq. **(2)**).

A comparison of the band positions assigned to the β-$CoMoO_4$, β-$Co_{0.7}Fe_{0.3}MoO_{12}$ and β-$FeMoO_4$ phases in the final Raman spectra (600 °C) of FSP-Co, FSP-Fe and FSP-U revealed a shift towards lower wavenumbers for FSP-Fe and FSP-U (**see SI section 6.2**). This supports that less β-$Co_{0.7}Fe_{0.3}MoO_{12}$ was formed in the case of FSP-Co, which is additionally indicated by the lowest amount of crystalline β-$CoMoO_4$/ β-$Co_{0.7}Fe_{0.3}MoO_4$ detected by XRD in the final state of FSP-Co (~ 59 wt%) compared to FSP-Fe (~ 67 wt%) and FSP-U (~ 87 wt%). Hence, these results are in line with the beneficial and thus promoting role of β-$Co_{0.7}Fe_{0.3}MoO_{12}$ discussed in literature with respect to selective propylene oxidation.[27, 65-66] According to this, β-$Co_{0.7}Fe_{0.3}MoO_{12}$ improves the catalytic performance by facilitating and moderating electron and oxygen mobility, thus increasing the efficiency of the Mars-van Krevelen mechanism.[65, 67]

Even though FSP-Co and FSP-Fe revealed a rather similar phase ensemble, crystalline Co_3O_4 was only detected in FSP-Co. This may have led to the poorest catalytic performance in the herein compared 4-component systems in selective isobutene oxidation. Co_3O_4 is typically used as a total oxidation catalyst,[68] and is also claimed to perform unselective in propylene oxidation.[69] Moreover, FSP-Co exhibited the initially highest amount of Mo^{6+} in octahedral coordination, which indicates that the previously discussed tendency of γ-Bi_2MoO_6 towards total oxidation products is mainly attributed to the presence of MoO_6 octahedra, as also present in α-$CoMoO_4$ or MoO_3. This is in accordance with the site isolation principle by Callahan and Grasselli, who postulated that isolated lattice oxygen groupings that contain more than five adjacent oxygens lead to unselective CO and CO_2 formation in selective propylene oxidation.[9, 70]

3.3 Phase interplay and effect on catalytic performance in Bi-Mo-Co-Fe-O systems

The comparison of catalytic activity, selectivity and structure of FSP-Co, FSP-Fe and FSP-U revealed pronounced differences in terms of initial metal oxide phase composition, their transformations during reaction, and synergistic effects between metal oxide phases. The initial elemental composition of the catalysts plays a crucial role and the corresponding crystalline phases formed probably also determine the surface structure. Notably, first studies addressing both the bulk and surface structure in such complex multi-component catalysts revealed similar elemental and metal oxide phase composition.[21, 71] Therefore, the bulk structure can be used as a first approximation for its influence on the surface structure, as both are expected to be strongly interlinked and both properties relevant.

While FSP-U performed best in terms of high, controllable isobutene conversion, showing highest methacrolein selectivity, FSP-Co and FSP-Fe were less selective but extremely active. This high activity is most likely attributed to the comparably low molybdenum content (< 50 mol%) and the resulting tendency to form single metal oxide phases (*e.g.*, Fe_3O_4, Co_3O_4, Bi_2O_3).

In particular, the Fe^{3+}/Fe^{2} redox couple is suggested to improve lattice oxygen transport through the catalyst, thus playing a crucial role in the catalytic cycle. The Fe^{3+} to Fe^{2+} reduction detected in FSP-U correlated with a decrease in catalytic activity, while highly active FSP-Co and FSP-Fe contained crystalline Fe_3O_4 and thus a constant supply of the iron redox couple and easily accessible oxygen during the whole TPRxn experiment. Consequently, only a certain Fe^{3+}/Fe^{2+} ratio seems to be beneficial for good catalytic performance. A similar observation was reported by Engeldinger *et al.*,[53] who investigated structural changes of mixed molybdate catalysts in propylene ammoxidation. Moreover, it was assumed that Fe^{2+} and Fe^{3+} can be stabilized within the β-$CoMoO_4$ and α-$Bi_2Mo_3O_{12}$, optimizing the Fe^{3+}/Fe^{2+} redox cycle.[53, 72] In this context, we

found an improving effect on catalytic performance of both, β-$Co_{0.7}Fe_{0.3}MoO_{12}$ and $Bi_3FeMo_2O_{12}$, that is in line with earlier observations during propylene oxidation.[73] However, $Bi_3FeMo_2O_{12}$ was only beneficial if present in rather low amounts and/or simultaneously with α-$Bi_2Mo_3O_{12}$, as in the case of FSP-U. Notably, α-$Bi_2Mo_3O_{12}$ was solely detected in FSP-U, while FSP-Co and FSP-Fe both showed the formation of γ-Bi_2MoO_6 during reaction. This indicates a higher tendency towards total oxidation *via* oxygen from $[Bi_2O_2]^{2+}$ layers within the γ-Bi_2MoO_6 structure, as also supported by Sprenger *et al.*[16]. Since γ-Bi_2MoO_6 was only observed upon ignition of the reaction, its formation might be directly correlated to the simultaneous transformation of α-$CoMoO_4$ to β-$CoMoO_4$. Such a transformation from the α- to β-$CoMoO_4$ phase, and thus a change in Mo^{6+} coordination, is in line with previous *ex situ* observations before and after selective isobutene or propylene oxidation.[23, 33] Here, this transformation with simultaneous presence of Bi_2O_3 occurred only in the cases of FSP-Co and FSP-Fe, which both contained less than 50 mol% molybdenum and thus a lower Mo/Bi ratio.

In general, these two catalysts showed similar behaviour in terms of (constant) high catalytic activity including high oxygen consumption, but FSP-Fe exhibited a higher methacrolein selectivity. Since also their complex phase ensemble was very similar, mainly differing in distinct phase amounts and the presence of crystalline Co_3O_4, which was only found in FSP-Co, Co_3O_4 might act unselectively in isobutene oxidation to methacrolein. As mentioned above, such single metal oxide formations in FSP-Co (*i.e.* Co_3O_4) and FSP-Fe (*i.e.* Fe_3O_4) directly correlated with a high cobalt or iron (40 mol%) and comparably low molybdenum content (35 mol%), consequently forming less molybdates. Vice versa, Stehle *et al.*[27] investigated a Bi-Mo-Co-Fe-O catalyst containing more than 50 mol% molybdenum (~ 60 mol%), that tended to form increased amounts of MoO_3 instead, acting unselectively during propylene oxidation. This illustrates the impact of

initial elemental ratios on phase formations and finally explains the relevance for multicomponent bismuth molybdate based catalysts to comprise 50-55% molybdenum. So far, this was only stated in patent descriptions, as reviewed by Moro-Oka and Ueda[4], without further justification and related structural insights into the resulting catalysts.

Obviously, phase interactions seem to have a predominant effect on catalytic performance in the 4-compoment systems. As illustrated in **Figure 11**, several phases (*e.g.*, α- and β-$CoMoO_4$, β-$Co_{0.7}Fe_{0.3}MoO_4$ or $Bi_3FeMo_2O_{12}$,) were found in each catalyst with partly similar amounts, still leading to different catalytic performance in terms of selective methacrolein formation and unselective total oxidation to CO and CO_2. This was mainly attributed to their synergistic interplay with different additional phases (*e.g.*, α-$Bi_2Mo_3O_{12}$, γ-Bi_2MoO_6, Co_3O_4). Consequently, the properties within defect scheelite structured α-$Bi_2Mo_3O_{12}$ and $Bi_3FeMo_2O_{12}$[74] contribute to high methacrolein selectivity, while the simultaneous presence of γ-Bi_2MoO_6 and Fe_3O_4 significantly enhanced both isobutene and oxygen conversion due to their properties of enabling fast oxygen transport through the lattice. The unselective role of Co_3O_4 can be traced back to its tendency of forming electrophilic oxygen species within the catalytic cycle.[75] Thus, this underlines that previously discussed activity and selectivity trends of model systems (*e.g.*, 2-component Bi-Mo-O)[12, 14-16, 19-20] aiming for a basic knowledge of the catalyst's working principles have to be further elaborated by considering phase cooperation in more active, selective and thus more application-related systems. This should be further complemented by investigations of the catalyst surface layer, which is equally important to the bulk *operando* methods presented in this work. Moreover, such complementary insights can contribute to a revised understanding of the particle model for Bi-Mo-Co-Fe-oxides. Wolfs *et al.* proposed a core-shell like model with a bismuth molybdate surface layer,[76] which appears oversimplified based on the herein discussed results.

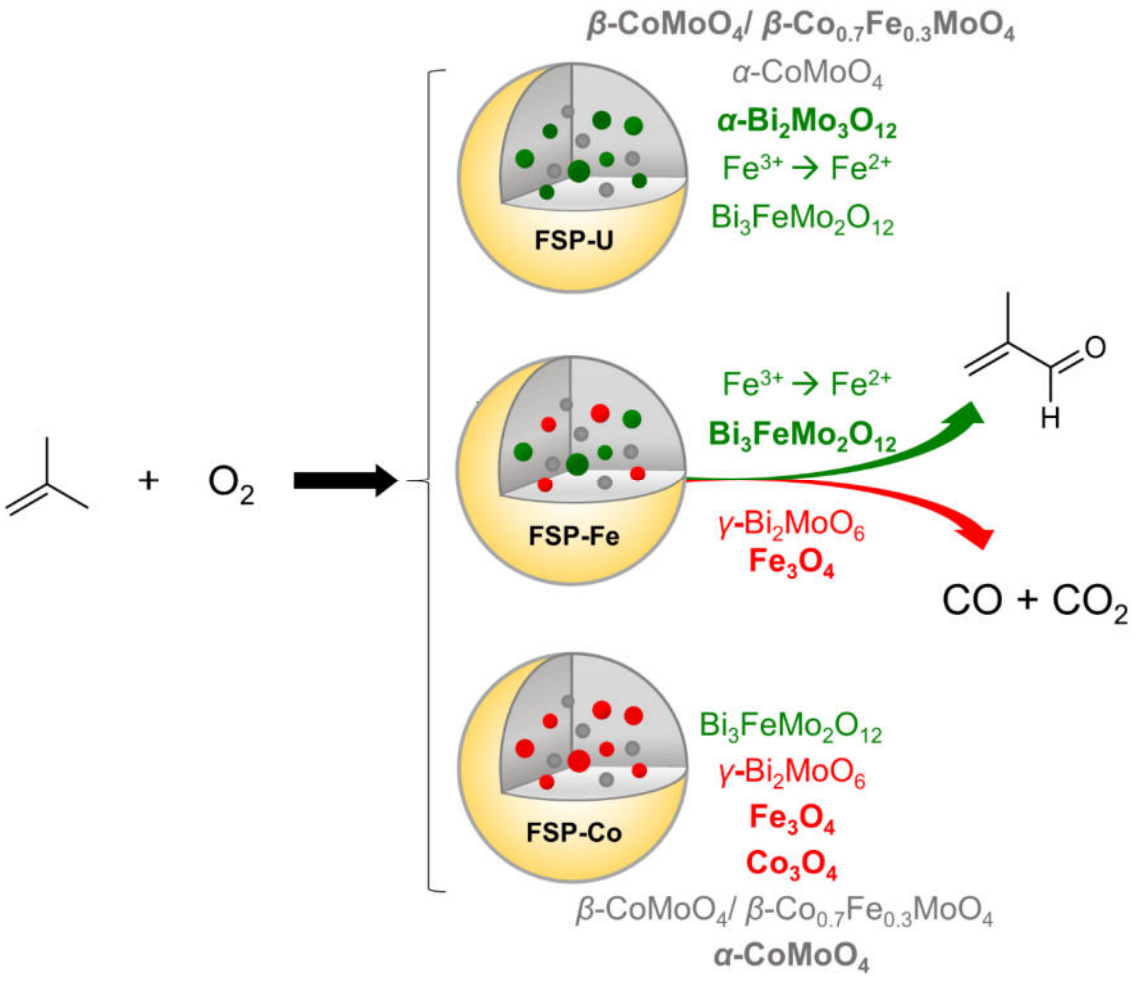

Figure 11. Schematic illustration of metal oxide phase cooperation within FSP-U (top), FSP-Fe (middle) and FSP-Co (bottom) during the selective oxidation of isobutene. Green: Metal oxide phases favouring the selective reaction pathway (MAC formation). Red: Metal oxide phases favouring the unselective reaction pathway (CO and CO_2 formation). Grey: Main phases detected in all three catalyst compositions. Bold: Main phases in relation to other catalyst compositions.

4 Conclusion

Three FSP-prepared Bi-Mo-Co-Fe-O catalysts differing in elemental composition were investigated during selective isobutene oxidation by the means of integral lab-reactor testing and complementary *operando* XAS, synchrotron XRD and Raman spectroscopy. The combination of conventional and advanced spectroscopic tools was crucial to investigate such complex catalyst compositions qualitatively and quantitatively. In this context, several phases could not be detected with lab XRD but required synchrotron XRD, underlining its high potential for unravelling such complex mixed metal oxides due to the high S/N ratio and small instrumental line broadening. In contrast, other phases (*e.g.*, isostructural β-$CoMoO_4$ and β-$FeMoO_4$) were hard to distinguish even by synchrotron XRD, but showed different band positions in Raman spectroscopy, thus pointing out the relevance of using complementary characterization techniques. In combination with the *operando* characterization approach, we could correlate the observed differences in terms of catalytic performance with distinct metal oxide phases in each system. These in turn were directly influenced by the metal ratios chosen for catalyst synthesis, with the molybdenum content being a crucial value, probably also inducing strongly different surface structures of the catalysts.

The two catalysts containing less than 50 mol% molybdenum (FSP-Co, FSP-Fe) showed particularly single metal oxide formation (*i.e.*, Fe_3O_4, Co_3O_4, Bi_2O_3) that resulted in very high catalytic activity involving high oxygen consumption. This was mainly attributed to the formation of γ-Bi_2MoO_6 upon ignition of the reaction and its phase interplay with constantly present Fe_3O_4. In contrast, a molybdenum content of 50 mol% (FSP-U) resulted in more controllable activity, by preferential formation of molybdate structures (*i.e.*, α-$Bi_2Mo_3O_{12}$ and $Fe_2Mo_3O_{12}$), which enabled *e.g.*, (nearly) full Fe^{3+} to Fe^{2+} reduction during TPRxn. Additionally, rather synergistic effects between the metal oxide phases in the 4-component systems than the surface area were found to

influence catalytic performance strongly. The simultaneous presence of β-$CoMoO_4$/ β-$Co_{0.7}Fe_{0.3}MoO_4$, α-$Bi_2Mo_3O_{12}$ and $Bi_3FeMo_2O_{12}$ observed in FSP-U resulted in best catalytic performance during selective isobutene oxidation, which is in good agreement with previous trends discussed in olefin oxidation literature.[4, 23, 27] In contrast, the presence of β-$CoMoO_4$/ β-$Co_{0.7}Fe_{0.3}MoO_4$, γ-Bi_2MoO_6, $Bi_3FeMo_2O_{12}$ and Fe_3O_4 found in the activated state of FSP-Co and FSP-Fe led to significantly more active but also more unselective catalysts. Especially, the additional presence of Co_3O_4 in FSP-Co favoured the total oxidation of isobutene.

Overall, this systematic study of 4-component systems was an ideal starting point to derive structure-activity relationships in more complex systems and particularly investigate phase cooperation. The applied complementary and advanced synchrotron-based techniques were essential to deconvolute the various metal oxide phases and the corresponding complex phase interplay.

In future, such studies should be complemented by experiments with higher surface sensitivity (*e.g.*, *in situ*/*operando* DRIFTS, ETEM), higher time (*e.g.*, under transient conditions) as well as spatial resolution (*e.g.*, along the reactor, in one catalyst grain) to further understand the dynamics of the individual metal oxide phases or the role of possible reaction intermediates. Especially the surface dynamics are challenging to monitor under working conditions due to both the heterogeneous metal oxide phase mixtures and experimental limitations. Hence, future surface studies (*e.g.*, XPS, SEM-EDX) should start with simplified conditions and start from model systems, similar to the approach chosen for the complementary bulk characterization but also move step by step to more complex Bi-Mo-Co-Fe-oxides. This would allow to further deepen the understanding of the interdependency between surface and bulk structure of mixed metal oxides in the long term.

ASSOCIATED CONTENT

Supporting Information

The following file is available free of charge.

"Supporting information: Additional material properties, experimental details, information on data analysis, including additional testing and characterization (XRD, XAS, Raman spectroscopy) results (PDF)"

AUTHOR INFORMATION

Corresponding Author

*grunwaldt@kit.edu

Present Addresses

† T.L. Sheppard: Institute of Chemical Technology, Leipzig University, 04103 Leipzig, Germany

Funding Sources

SOLEIL/ ANR: ANR-10-EQPX-45

ESRF: BM01

Deutsche Forschungsgemeinschaft: INST 121384/73-1

Acknowledgements

We acknowledge SOLEIL for provision of synchrotron radiation facilities and we would like to thank Dr. Camille La Fontaine and Dr. Valérie Briois for assistance in using beamline ROCK for XAS measurements (proposal number 20201100). The work at ROCK was supported by a public grant overseen by the French National Research Agency (ANR) as part of the "Investissements d'Avenir" program (reference: ANR-10-EQPX-45). We acknowledge the European Synchrotron Radiation Facility for provision of synchrotron radiation facilities and we would like to thank Dr. Charles McMonagle for assistance in using beamline BM01 for XRD measurements (proposal number CH-6051). We acknowledge KIT and DFG for financing the Raman spectrometer system (INST 121384/73-1). We thank Dr. Bidyut Bikash Sarma, Dr. Birte Wollak and Mariam Schulte for assistance during beamtimes, Dr. Thomas Bergfeldt (IAM-AWP, KIT) for ICP-OES analysis, Dr. Michael Zimmermann (IKFT, KIT) for SEM-EDX measurements and Simon Falkner (AOC, KIT) for N_2 physisorption experiments.

References

1. Arntz, D.; Fischer, A.; Höpp, M.; Jacobi, S.; Sauer, J.; Ohara, T.; Sato, T.; Shimizu, N.; Schwind, H., Acrolein and methacrolein. In *Ullmann's encyclopedia of industrial chemistry*, Wiley-VCH: Weinheim, 2007; pp 329-346.
2. Haber, J., Fundamentals of hydrocarbon oxidation. In *Handbook of Heterogeneous Catalysis*, Ertl, G.; Knözinger, H.; Schüth, F.; Weitkamp, J., Eds. Wiley-VCH: Weinheim, 2008; pp 3359-3384.
3. Grasselli, R. K.; Burrington, J. D., Oxidation of Low-Molecular-Weight Hydrocarbons. In *Handbook of Heterogeneous Catalysis*, Ertl, G.; Knözinger, H.; Schüth, F.; Weitkamp, J., Eds. Wiley-VCH: Weinheim, 2008; pp 3479-3489.
4. Moro-Oka, Y.; Ueda, W., Multicomponent bismuth molybdate catalyst: A highly functionalized catalyst system for the selective oxidation of olefin. *Adv. Catal.* **1994,** *40*, 233-273.
5. Brazdil, J. F., A critical perspective on the design and development of metal oxide catalysts for selective propylene ammoxidation and oxidation. *Appl. Catal., A* **2017,** *543*, 225-233.
6. Grasselli, R. K., Fundamental principles of selective heterogeneous oxidation catalysis. *Top. Catal.* **2002,** *21* (1-3), 79-88.
7. Callahan, J. L.; Grasselli, R. K.; Milberger, E. C.; Strecker, H. A., Oxidation and ammoxidation of propylene over bismuth molybdate catalyst. *Ind. Eng. Chem. Prod. Res. Develop.* **1970,** *9* (2), 134-142.
8. Bell, A. T., Insights into the mechanism and kinetics of propene oxidation and ammoxidation over bismuth molybdate catalysts derived from experiments and theory. *J. Catal.* **2022,** *408*, 436-452.
9. Grasselli, R. K., Site isolation and phase cooperation: Two important concepts in selective oxidation catalysis: A retrospective. *Catal. Today* **2014,** *238*, 10-27.
10. Keulks, G. W.; Krenzke, L. D.; Notermann, T. M., Selective oxidation of propylene. *Adv. Catal.* **1979,** *27*, 183-225.
11. Sprenger, P.; Kleist, W.; Grunwaldt, J.-D., Recent Advances in Selective Propylene Oxidation over Bismuth Molybdate Based Catalysts: Synthetic, Spectroscopic, and Theoretical Approaches. *ACS Catal.* **2017,** *7* (9), 5628-5642.
12. Carson, D.; Coudurier, G.; Forissier, M.; Védrine, J. C.; Laarif, A.; Theobald, F., Synergy effects in the catalytic properties of bismuth molybdates. *J. Chem. Soc., Faraday Trans. 1* **1983,** *79* (8), 1921-1929.
13. Monnier, J. R.; Keulks, G. W., The catalytic oxidation of propylene: IX. The kinetics and mechanism over β-$Bi_2Mo_2O_9$. *J. Catal.* **1981,** *68* (1), 51-66.
14. Brazdil, J. F.; Suresh, D. D.; Grasselli, R. K., Redox kinetics of bismuth molybdate ammoxidation catalysts. *J. Catal.* **1980,** *66* (2), 347-367.
15. Schuh, K.; Kleist, W.; Høj, M.; Trouillet, V.; Beato, P.; Jensen, A. D.; Grunwaldt, J.-D., Bismuth molybdate catalysts prepared by mild hydrothermal synthesis: Influence of pH on the selective oxidation of propylene. *Catalysts* **2015,** *5* (3), 1554-1573.
16. Sprenger, P.; Stehle, M.; Gaur, A.; Gänzler, A. M.; Gashnikova, D.; Kleist, W.; Grunwaldt, J.-D., Reactivity of Bismuth Molybdates for Selective Oxidation of Propylene Probed by Correlative Operando Spectroscopies. *ACS Catal.* **2018,** *8* (7), 6462-6475.

17. Ueda, W.; Moro-Oka, Y.; Ikawa, T., Promotion effect of iron for the multicomponent bismuth molybdate catalysts as revealed by $^{18}O_2$ tracer. *Chem. Lett.* **1982,** *11* (9), 1365-1368.
18. Bing, Z.; Pei, S.; Shishan, S.; Xiexian, G., Cooperation between the α and γ phases of bismuth molybdate in the selective oxidation of propene. *J. Chem. Soc., Faraday Trans.* **1990,** *86* (18), 3145-3150.
19. Soares, A. P. V.; Dimitrov, L. D.; de Oliveira, M. C.-R. A.; Hilaire, L.; Portela, M. F.; Grasselli, R. K., Synergy effects between β and γ phases of bismuth molybdates in the selective catalytic oxidation of 1-butene. *Appl. Catal., A* **2003,** *253* (1), 191-200.
20. Le, M. T.; Van Well, W. J.; Stoltze, P.; Van Driessche, I.; Hoste, S., Synergy effects between bismuth molybdate catalyst phases (Bi/Mo from 0.57 to 2) for the selective oxidation of propylene to arcrolein. *Appl. Catal., A* **2005,** *282* (1-2), 189-194.
21. Amakawa, K.; Mauss, J. M.; Müller, P.; Hinrichsen, B.; Hirth, S.; Bader, A.; Price, S. W. T.; Jacques, S. D.; Macht, J., Architecture of industrial Bi-Mo-Co-Fe-K-O propene oxidation catalysts. *Science advances* **2023,** *9*.
22. Udalova, O.; Shashkin, D.; Shibanova, M.; Krylov, O., Action of Co-Mo-Bi-Fe-Sb-K catalysts in the partial oxidation of propylene to acrolein: 1. The composition dependence of activity and selectivity. *Kinet. Catal.* **2005,** *46* (4), 535-544.
23. Shashkin, D.; Udalova, O.; Shibanova, M.; Krylov, O., The mechanism of action of a multicomponent Co-Mo-Bi-Fe-Sb-K-O catalyst for the partial oxidation of propylene to acrolein: II. Changes in the phase composition of the catalyst under reaction conditions. *Kinet. Catal.* **2005,** *46* (4), 545-549.
24. Sprenger, P.; Sheppard, T. L.; Suuronen, J.-P.; Gaur, A.; Benzi, F.; Grunwaldt, J.-D., Structural Evolution of Highly Active Multicomponent Catalysts for Selective Propylene Oxidation. *Catalysts* **2018,** *8* (9), 356-376.
25. Wachs, I. E.; Routray, K., Catalysis Science of Bulk Mixed Oxides. *ACS Catal.* **2012,** *2* (6), 1235-1246.
26. Klag, L.; Sheppard, T. L.; Grunwaldt, J.-D., An Advanced Characterization Toolbox for Selective Olefin Oxidation Catalysts. *ChemCatChem* **2023,** *15* (3).
27. Stehle, M.; Gaur, A.; Weber, S.; Sheppard, T. L.; Thomann, M.; Fischer, A.; Grunwaldt, J.-D., Complementary operando insights into the activation of multicomponent selective propylene oxidation catalysts. *J. Catal.* **2022,** *408*, 339-355.
28. Krabetz, R., Selektive katalytische Oxidation von Olefinen. *Chemie-Ing.-Techn.* **1974,** *46. Jahrg.* (4), 1029-1041.
29. Carrazán, S. R. G.; Martín, C.; Rives, V.; Vidal, R., Selective oxidation of isobutene to methacrolein on multiphasic molybdate-based catalysts. *Appl. Catal., A* **1996,** *135* (1), 95-123.
30. Breiter, S.; Lintz, H.-G., Partial oxidation of isobutene to methacrolein on BiW/FeCoMoK mixed oxide catalysts. *Chem. Eng. Sci.* **1995,** *50* (5), 785-791.
31. Wang, F.; Wang, G.; Niu, X., Study on the Effect of Nickel Doping on Mo-Bi Based Catalyst for Selective Oxidation of Isobutene to Methacrolein. *Int. J. Chem. React. Eng.* **2016,** *14* (1), 105-112.
32. Moens, L.; Ruiz, P.; Delmon, B.; Devillers, M., Evaluation of the role played of bismuth molybdates in $Bi_2Sn_2O_7$-MoO_3 catalysts used for partial oxidation of isobutene to methacrolein. *Appl. Catal., A* **1999,** *180*, 299-315.
33. Udalova, O. V.; Shashkin, D. P.; Shibanova, M. D.; Krylov, O. V., Changes in the phase composition of a multicomponent Co-Mo-Bi-Fe-Sb-K-O catalyst under conditions of the partial

oxidation of isobutylene to methacrolein: A comparison with the oxidation of propylene to acrolein. *Kinet. Catal.* **2008,** *49* (3), 407-412.
34. Mädler, L.; Pratsinis, S. E., Bismuth oxide nanoparticles by flame spray pyrolysis. *J. Am. Ceram. Soc.* **2002,** *85* (7), 1713-1718.
35. Schuh, K.; Kleist, W.; Høj, M.; Trouillet, V.; Jensen, A. D.; Grunwaldt, J.-D., One-step synthesis of bismuth molybdate catalysts via flame spray pyrolysis for the selective oxidation of propylene to acrolein. *Chem. Commun.* **2014,** *50* (97), 15404-15406.
36. Brunauer, S.; Emmett, P. H.; Teller, E., Adsorption of gases in multimolecular layers. *J. Am. Chem. Soc.* **1938,** *60* (2), 309-319.
37. Grunwaldt, J.-D.; Caravati, M.; Hannemann, S.; Baiker, A., X-ray absorption spectroscopy under reaction conditions: suitability of different reaction cells for combined catalyst characterization and time-resolved studies. *Phys. Chem. Chem. Phys.* **2004,** *6* (11), 3037-3047.
38. Dyadkin, V.; Pattison, P.; Dmitriev, V.; Chernyshov, D., A new multipurpose diffractometer PILATUS@ SNBL. *J. Synchrotron Radiat.* **2016,** *23* (3), 825-829.
39. Coelho, A. A., TOPAS and TOPAS-Academic: an optimization program integrating computer algebra and crystallographic objects written in C++. *J. Appl. Crystallogr.* **2018,** *51* (1), 210-218.
40. Briois, V.; La Fontaine, C.; Belin, S.; Barthe, L.; Moreno, T.; Pinty, V.; Carcy, A.; Girardot, R.; Fonda, E., ROCK: the new Quick-EXAFS beamline at SOLEIL. *J. Phys. Conf. Ser.* **2016,** *712* (1), 012149.
41. La Fontaine, C.; Belin, S.; Barthe, L.; Roudenko, O.; Briois, V., ROCK: A Beamline Tailored for Catalysis and Energy-Related Materials from ms Time Resolution to µm Spatial Resolution. *Synchrotron Radiat. News* **2020,** *33* (1), 20-25.
42. Lesage, C.; Devers, E.; Legens, C.; Fernandes, G.; Roudenko, O.; Briois, V., High pressure cell for edge jumping X-ray absorption spectroscopy: Applications to industrial liquid sulfidation of hydrotreatment catalysts. *Catal. Today* **2019,** *336*, 63-73.
43. Ravel, B.; Newville, M., ATHENA, ARTEMIS, HEPHAESTUS: data analysis for X-ray absorption spectroscopy using IFEFFIT. *J. Synchrotron Radiat.* **2005,** *12* (4), 537-541.
44. Zhang, L.; Liu, D.; Yang, B.; Zhao, J., Investigations of the mechanisms and kinetics leading to a loss of molybdenum from bismuth molybdate catalysts. *Appl. Catal., A* **1994,** *117* (2), 163-171.
45. Raun, K. V.; Johannessen, J.; McCormack, K.; Appel, C. C.; Baier, S.; Thorhauge, M.; Høj, M.; Jensen, A. D., Modeling of the molybdenum loss in iron molybdate catalyst pellets for selective oxidation of methanol to formaldehyde. *Chem. Eng. J.* **2019,** *361*, 1285-1295.
46. Sparks, T. D.; Gurlo, A.; Bekheet, M. F.; Gaultois, M. W.; Cherkashinin, G.; Laversenne, L.; Clarke, D. R., High-temperature structure of Co_3O_4: Understanding spinel inversion using in situ and ex situ measurements. *Phys. Rev. B* **2019,** *99* (10).
47. Peck, T. C.; Roberts, C. A.; Reddy, G. K., Contrasting Effects of Potassium Addition on M_3O_4 (M = Co, Fe, and Mn) Oxides during Direct NO Decomposition Catalysis. *Catalysts* **2020,** *10* (5).
48. D'Ippolito, V.; Andreozzi, G. B.; Bersani, D.; Lottici, P. P., Raman fingerprint of chromate, aluminate and ferrite spinels. *J. Raman Spectrosc.* **2015,** *46* (12), 1255-1264.
49. Trunschke, A., 11 Synthesis of Solid Catalysts. In *Chemical Energy Storage*, 2022; pp 301-368.

50. Payen, E.; Dhamelincourt, M.; Dhamelincourt, P.; Grimblot, J.; Bonnelle, J., Study of Co (or Ni)-Mo oxide phase transformation and hydrodesulfurization catalysts by Raman microprobe equipped with new cells. *Appl. Spectrosc.* **1982,** *36* (1), 30-37.
51. Costa, R. K. S.; Teles, S. C.; Siqueira, K. P. F., The relationship between crystal structures and thermochromism in $CoMoO_4$. *Chem. Pap.* **2021,** *75* (1), 237-248.
52. Saleem, S. S., Infrared and Raman spectroscopic studies of the polymorphic forms of nickel, cobalt and ferric molybdates. *Infrared Phys.* **1987,** *27* (5), 309-315.
53. Engeldinger, J.; Radnik, J.; Kreyenschulte, C.; Devred, F.; Gaigneaux, E. M.; Fischer, A.; Zanthoff, H. W.; Bentrup, U., Probing the Structural Changes and Redox Behavior of Mixed Molybdate Catalysts under Ammoxidation Conditions: An Operando Raman Spectroscopy Study. *ChemCatChem* **2016,** *8* (5), 976-983.
54. Rodriguez, J. A.; Chaturvedi, S.; Hanson, J. C.; Albornoz, A.; Brito, J. L., Electronic properties and phase transformations in CoMoO4 and NiMoO4: XANES and time-resolved synchrotron XRD studies. *J. Phys. Chem. B* **1998,** *102* (8), 1347-1355.
55. Gaur, A.; Stehle, M.; Raun, K. V.; Thrane, J.; Jensen, A. D.; Grunwaldt, J.-D.; Høj, M., Structural dynamics of an iron molybdate catalyst under redox cycling conditions studied with in situ multi edge XAS and XRD. *Phys. Chem. Chem. Phys.* **2020,** *22* (20), 11713-11723.
56. Kongmark, C.; Coulter, R.; Cristol, S.; Rubbens, A.; Pirovano, C.; Löfberg, A.; Sankar, G.; Van Beek, W.; Bordes-Richard, E.; Vannier, R.-N. l., A comprehensive scenario of the crystal growth of γ-Bi_2MoO_6 catalyst during hydrothermal synthesis. *Cryst. Growth Des.* **2012,** *12* (12), 5994-6003.
57. Kongmark, C.; Martis, V.; Pirovano, C.; Löfberg, A.; Van Beek, W.; Sankar, G.; Rubbens, A.; Cristol, S.; Vannier, R.-N.; Bordes-Richard, E., Synthesis of γ-Bi_2MoO_6 catalyst studied by combined high-resolution powder diffraction, XANES and Raman spectroscopy. *Catal. Today* **2010,** *157* (1-4), 257-262.
58. Eda, K.; Uno, Y.; Nagai, N.; Sotani, N.; Whittingham, M. S., Crystal structure of cobalt molybdate hydrate $CoMoO_4 \cdot nH_2O$. *J. Solid State Chem.* **2005,** *178* (9), 2791-2797.
59. Sleight, A. W.; Chamberland, B. L.; Weiher, J. F., Magnetic, Moessbauer, and structural studies on three modifications of $FeMoO_4$. *Inorg. Chem.* **1968,** *7* (6), 1093-1098.
60. Jeitschko, W.; Sleight, A.; McClellan, W.; Weiher, J., A comprehensive study of disordered and ordered scheelite-related $Bi_3(FeO_4)(MoO_4)_2$. *Acta Crystallogr. Sect. B: Struct. Sci.* **1976,** *32* (4), 1163-1170.
61. Hardcastle, F. D.; Wachs, I. E., Molecular structure of molybdenum oxide in bismuth molybdates by Raman spectroscopy. *J. Phys. Chem.* **1991,** *95* (26), 10763-10772.
62. Jung, J. C.; Kim, H.; Choi, A. S.; Chung, Y.-M.; Kim, T. J.; Lee, S. J.; Oh, S.-H.; Song, I. K., Effect of pH in the preparation of γ-Bi_2MoO_6 for oxidative dehydrogenation of n-butene to 1, 3-butadiene: Correlation between catalytic performance and oxygen mobility of γ-Bi_2MoO_6. *Catal. Commun.* **2007,** *8* (3), 625-628.
63. Le, M. T.; Bac, L. H.; Van Driessche, I.; Hoste, S.; Van Well, W. J., The synergy effect between gamma and beta phase of bismuth molybdate catalysts: Is there any relation between conductivity and catalytic activity? *Catal. Today* **2008,** *131* (1-4), 566-571.
64. Krenzke, L. D.; Keulks, G. W., The catalytic oxidation of propylene: VIII. An investigation of the kinetics over $Bi_2Mo_3O_{12}$, Bi_2MoO_6, and $Bi_3FeMo_2O_{12}$. *J. Catal.* **1980,** *64* (2), 295-302.
65. He, D.-H.; Ueda, W.; Moro-Oka, Y., Promotion effect of molybdate support on $Bi_2Mo_3O_{12}$ catalyst in the selective oxidation of propylene. *Catal. Lett.* **1992,** *12* (1-3), 35-44.

66. Ponceblanc, H.; Millet, J.-M. M.; Coudurier, G.; Védrine, J. C., Synergy effect of multicomponent Co, Fe, and Bi molybdates in propene partial oxidation. In *Catalytic Selective Oxidation*, Oyama, S. T.; Hightower, J. W., Eds. ACS Publications: Washington, DC, 1993; pp 262-272.
67. Millet, J.-M. M.; Ponceblanc, H.; Coudurier, G.; Herrmann, J. M.; Védrine, J. C., Study of multiphasic molybdate-based catalysts: II. Synergy effect between bismuth molybdates and mixed iron and cobalt molybdates in mild oxidation of propene. *J. Catal.* **1993,** *142* (2), 381-391.
68. Solsona, B.; Davies, T. E.; Garcia, T.; Vázquez, I.; Dejoz, A.; Taylor, S. H., Total oxidation of propane using nanocrystalline cobalt oxide and supported cobalt oxide catalysts. *Appl. Catal., B* **2008,** *84* (1-2), 176-184.
69. Haber, J.; Turek, W., Kinetic studies as a method to differentiate between oxygen species involved in the oxidation of propene. *J. Catal.* **2000,** *190* (2), 320-326.
70. Callahan, J.; Grasselli, R., A selectivity factor in vapor-phase hydrocarbon oxidation catalysis. *AlChE J.* **1963,** *9* (6), 755-760.
71. Sprenger, P.; Stehle, M.; Gaur, A.; Weiß, J.; Brueckner, D.; Zhang, Y.; Garrevoet, J.; Suuronen, J.-P.; Thomann, M.; Fischer, A.; Grunwaldt, J.-D.; Sheppard, T. L., Chemical Imaging of Mixed Metal Oxide Catalysts for Propylene Oxidation: From Model Binary Systems to Complex Multicomponent Systems. *ChemCatChem* **2021,** *13* (10), 2483-2493.
72. Benaichouba, B.; Bussiere, P.; Védrine, J. C., In-situ Mössbauer spectroscopic study of iron site evolution in iron and cobalt molybdates catalysts in propene oxidation reaction conditions. *Appl. Catal., A* **1995,** *130* (1), 31-45.
73. Legendre, O.; Jaeger, P.; Brunelle, J., Strong evidence of synergetic effects between cobalt, iron and bismuth molybdates in propene oxidation to acrolein. In *Stud. Surf. Sci. Catal.*, Ruiz, P.; Delmon, B., Eds. Elsevier: 1992; Vol. 72, pp 387-398.
74. Brazdil, J. F., Scheelite: a versatile structural template for selective alkene oxidation catalysts. *Cat. Sci. Tec.* **2015,** *5* (7), 3452-3458.
75. Bielański, A.; Haber, J., Oxygen in catalysis on transition metal oxides. *Cat. Rev.: Sci. Eng.* **1979,** *19* (1), 1-41.
76. Wolfs, M.; Batist, P., The selective oxidation of 1-butene over a multicomponent molybdate catalyst. Influences of various elements on structure and activity. *J. Catal.* **1974,** *32* (1), 25-36.

Table of Contents graphic